

<sub>1</sub> Study of neutrino-nucleus interaction at around 1 GeV using  
<sub>2</sub> a 3D grid-structure neutrino detector, WAGASCI, muon  
<sub>3</sub> range detectors and magnetized spectrometer, Baby MIND,  
<sub>4</sub> at J-PARC neutrino monitor hall

<sub>5</sub> A. Bonnemaison, R. Cornat, L. Domine, O. Drapier, O. Ferreira, F. Gastaldi,  
<sub>6</sub> M. Gonin, J. Imber, M. Licciardi, F. Magniette, T. Mueller, L. Vignoli, and O. Volcy  
<sub>7</sub> *Ecole Polytechnique, IN2P3-CNRS, Laboratoire Leprince-Ringuet, Palaiseau,*  
<sub>8</sub> *France*

<sub>9</sub> S. Cao and T. Kobayashi

<sub>10</sub> *High Energy Accelerator Research Organization (KEK), Tsukuba, Ibaraki, Japan*

<sub>11</sub> M. Khabibullin, A. Khotjantsev, A. Kostin, Y. Kudenko, A. Mefodiev, O. Mineev,  
<sub>12</sub> S. Suvorov, and N. Yershov

<sub>13</sub> *Institute for Nuclear Research of the Russian Academy of Sciences, Moscow, Russia*

<sub>14</sub> B. Quilain

<sub>15</sub> *Kavli Institute for the Physics and Mathematics of the Universe (WPI), The*  
<sub>16</sub> *University of Tokyo Institutes for Advanced Study, University of Tokyo, Kashiwa,*  
<sub>17</sub> *Chiba, Japan*

<sub>18</sub> T. Hayashino, A. Hiramoto, A.K. Ichikawa, K. Nakamura, T. Nakaya, K Yasutome,  
<sub>19</sub> and K. Yoshida

<sub>20</sub> *Kyoto University, Department of Physics, Kyoto, Japan*

<sub>21</sub> Y. Azuma, J. Harada, T. Inoue, K. Kin, N. Kukita, S. Tanaka, Y. Seiya,  
<sub>22</sub> K. Wakamatsu, and K. Yamamoto

<sub>23</sub> *Osaka City University, Department of Physics, Osaka, Japan*

24 A. Blondel, F. Cadoux, Y. Favere, E. Noah, L. Nicola, and S. Parsa

25 *University of Geneva, Section de Physique, DPNC, Geneva, Switzerland*

26 N. Chikuma, F. Hosomi, T. Koga, R. Tamura, and M. Yokoyama

27 *University of Tokyo, Department of Physics, Tokyo, Japan*

28 Y. Hayato

29 *University of Tokyo, Institute for Cosmic Ray Research, Kamioka Observatory,*  
30 *Kamioka, Japan*

31 Y. Asada, K. Matsushita, A. Minamino, K. Okamoto, and D. Yamaguchi

32 *Yokohama National University, Faculty of Engineering, Yokohama, Japan*

33 December 14, 2017

## 34 **Contents**

|    |          |                                    |          |
|----|----------|------------------------------------|----------|
| 35 | <b>1</b> | <b>Introduction</b>                | <b>3</b> |
| 36 | <b>2</b> | <b>Experimental Setup</b>          | <b>4</b> |
| 37 | 2.1      | Wagasci modules . . . . .          | 5        |
| 38 | 2.1.1    | Detector . . . . .                 | 5        |
| 39 | 2.1.2    | Electronics . . . . .              | 8        |
| 40 | 2.1.3    | Water system . . . . .             | 9        |
| 41 | 2.2      | INGRID Proton module . . . . .     | 10       |
| 42 | 2.3      | Baby MIND . . . . .                | 11       |
| 43 | 2.3.1    | Magnet modules . . . . .           | 11       |
| 44 | 2.3.2    | Scintillator modules . . . . .     | 12       |
| 45 | 2.3.3    | Electronics . . . . .              | 14       |
| 46 | 2.3.4    | Pefromance check . . . . .         | 15       |
| 47 | 2.4      | Side muon range detector . . . . . | 16       |

|    |                                                                            |           |
|----|----------------------------------------------------------------------------|-----------|
| 48 | <b>3 Physics goals</b>                                                     | <b>18</b> |
| 49 | 3.1 Expected number of events . . . . .                                    | 19        |
| 50 | 3.2 Pseudo-monochromatic beam by using different off-axis fluxes . . . . . | 19        |
| 51 | 3.3 Subjects Wagasci can contribute . . . . .                              | 20        |
| 52 | <b>4 Status of J-PARC T59 experiment</b>                                   | <b>21</b> |
| 53 | <b>5 MC studies</b>                                                        | <b>23</b> |
| 54 | 5.1 Detector simulation . . . . .                                          | 23        |
| 55 | 5.1.1 Detector geometry . . . . .                                          | 24        |
| 56 | 5.1.2 Response of detector components . . . . .                            | 24        |
| 57 | 5.2 Track reconstruction . . . . .                                         | 25        |
| 58 | 5.3 Event selection . . . . .                                              | 25        |
| 59 | 5.4 Cross section measurements . . . . .                                   | 28        |
| 60 | <b>6 Standalone WAGASCI-module performances</b>                            | <b>30</b> |
| 61 | 6.1 Reconstruction algorithm . . . . .                                     | 32        |
| 62 | 6.1.1 Description . . . . .                                                | 32        |
| 63 | 6.1.2 Performances . . . . .                                               | 35        |
| 64 | 6.2 Background subtraction: the water-out module . . . . .                 | 39        |
| 65 | <b>7 Schedule</b>                                                          | <b>42</b> |
| 66 | <b>8 Requests</b>                                                          | <b>42</b> |
| 67 | 8.1 Neutrino beam . . . . .                                                | 42        |
| 68 | 8.2 Equipment request including power line . . . . .                       | 42        |

## 69 **1 Introduction**

70 The understanding of neutrino-nucleus interactions in the 1 GeV energy region is critical  
 71 for the success of accelerator-based neutrino oscillation experiments such as the T2K exper-  
 72 iment. Complicated multi-body effects of nuclei render this understanding difficult. The  
 73 T2K near detectors have been measuring these and significant progress has been achieved.  
 74 However, the understanding is still limited. One of the big factors preventing from full  
 75 understanding is the non-monochromatic neutrino beam spectrum. Measurements with  
 76 different but some overlapping beam spectra would greatly benefit to resolve the contrib-  
 77 ution from different neutrino energies. We, the Wagasci collaboration, proposes to study  
 78 the neutrino-nucleus interaction at the B2 floor of the neutrino monitor building, where  
 79 different neutrino spectra can be obtained due to the different off-axis position. Our exper-  
 80 imental setup contains 3D grid-structure plastic-scintillator detectors filled with water as  
 81 the neutrino interaction target (Wagasci modules), two side- and one downstream- muon

range detectors(MRD's). The 3D grid-structure and side-MRD's allows a measurement of wider-angle scattering than the T2K off-axis near detector (ND280). High water to scintillator material ratio enables the measurement of the neutrino interaction on water, which is highly desired for the T2K experiment because it's far detector, Super-Kamiokande, is composed of water. The MRD's consist of plastic scintillators and iron plates. The downstream-MRD, so called the Baby MIND detector, also works as a magnet and provides the charge identification capability as well as magnetic momentum measurement for high energy muons. The charge identification is essentially important to select antineutrino events in the antineutrino beam because contamination of the neutrino events is as high as 30%. Most of the detectors has been already constructed. The Wagasci modules have been commissioned as the J-PARC T59 experiment and the Baby MIND detector was commissioned at the CERN neutrino platform. Therefore, the collaboration will be ready to proceed to the physics data taking for the T2K beam time in January 2019. We will provide the cross sections of the charged current neutrino and antineutrino interactions on water with slightly higher neutrino energy than T2K ND280 with wide angler acceptance. When combined with ND280 measurements, our measurement would greatly improve the understanding of the neutrino interaction at around 1 GeV and contribute to reduce one of the most significant uncertainty of the T2K experiment.

## 2 Experimental Setup

Figure. 1 and 2 show a schematic view and a CAD drawing of the entire set of detectors. Central neutrino target detectors consist of two Wagasci modules and T2K INGRID proton module. Inside the Wagasci module, plastic scintillator bars are aligned as a 3D grid-like structure and spaces in the structure are filled with water for a water-in Wagasci module. T2K INGRID proton module is a full active neutrino target detector which is composed only with scintillator bars in its tracking region. The central detectors are surrounded by two side- and one downstream- muon range detectors(MRD's) The MRD's are used to select muon tracks from the charged-current (CC) interactions and to reject short tracks caused by neutral particles that originate mainly from neutrino interactions in material surrounding the central detector, like the walls of the detector hall, neutrons and gammas, or neutral-current (NC) interactions. The muon momentum can be reconstructed from its range inside the detector. The MRD's consist of plastic scintillators and iron plates. In addition, each of the iron plates of the downstream-MRD, so called the Baby MIND detector, is wound by a coil and can be magnetized. It provide the charge selection capability.

For all detectors, scintillation light in the scintillator bar is collected and transported to a photodetector with a wavelength shifting fiber (WLS fiber). The light is read out by a photodetector, Multi-Pixel Photon Counter (MPPC), attached to one end of the WLS fiber. The signal from the MPPC is read out by the dedicated electronics developed for the test experiment to enable bunch separation in the beam spill. The readout electronics is

120 triggered using the beam-timing signal from MR to synchronize to the beam. The beam-  
121 timing signal is branched from those for T2K, and will not cause any effect on the T2K  
122 data taking.

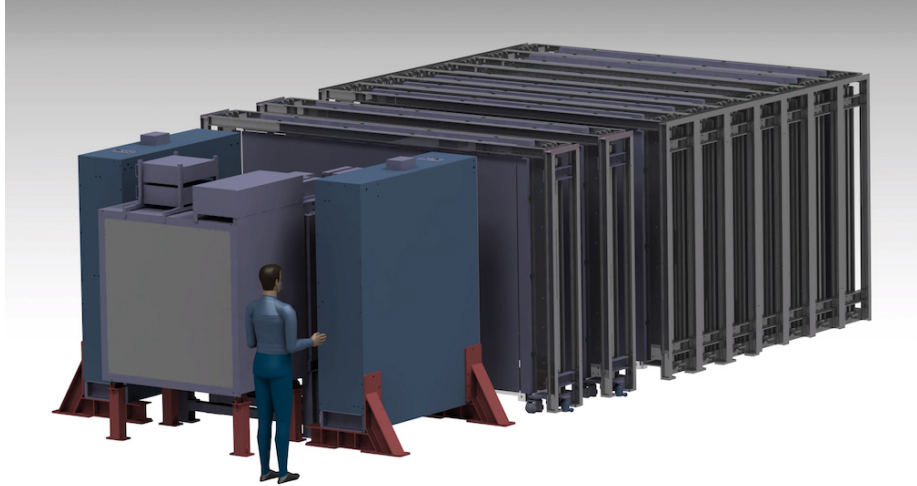


Figure 1: Schematic view of entire sets of detectors.

123 T2K adopted the off-axis beam method, in which the neutrino beam is intentionally  
124 directed 2.5 degrees away from SK producing a narrow band  $\nu_\mu$  beam. The off-axis near  
125 detector, ND280, is installed towards the SK direction in the B1 floor of the near detector  
126 hall of the J-PARC neutrino beam-line. We propose to install our detector in the B2 floor  
127 of the near detector hall, where the off-axis angle is similar but slightly different: 1.5 degree.  
128 The candidate detector position in the B2 floor is shown in Fig. 3. The expected neutrino  
129 energy spectrum at the candidate position is shown in Fig. 4.

## 130 2.1 Wagasci modules

### 131 2.1.1 Detector

132 The WAGASCI modules are mainly composed of 1280 plastic scintillator bars and a sur-  
133 rounding stainless steel tank as shown in Fig. 5. The total number of channels in one  
134 Wagasci module is 1280. The stainless steel tank is constructed by welding stainless steel  
135 plates, is sized as  $46 \times 125 \times 125 \text{ cm}^3$ , and weighs 0.5 ton.

136 One Wagasci module consists of 16 scintillator tracking planes, where each plane is an  
137 array of 80 scintillator bars fixed with ABS frames. The 40 bars, called parallel scintillators,  
138 are placed perpendicularly to the beam, and the other 40 bars, called grid scintillators, are  
139 placed in parallel to the beam with grid structure in the tracking plane as shown in Fig.

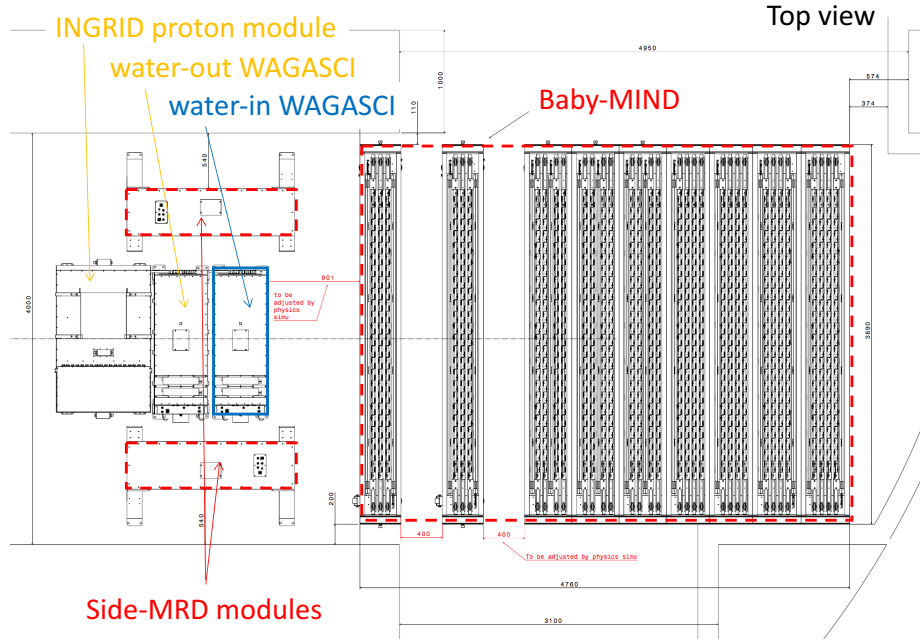


Figure 2: Top view of entire sets of detectors.

140 5. Thanks to the 3 D grid-like structure of the scintillator bars, the Wagasci module has  
 141  $4\pi$  angular acceptance for charged particles.

142 Thin plastic scintillator bars produced at Fermilab by extrusion method, mainly consists  
 143 of polystyrene and are surrounded by thin reflector including  $\text{TiO}_2$  (3 mm in thickness)  
 144 are used for the Wagasci modules to reduce the mass ratio of scintillator bars to water,  
 145 because neutrino interactions in the scintillator bars are a background for the cross section  
 146 measurements on  $\text{H}_2\text{O}$ . Each scintillator bar is sized as  $1020 \times 25 \times 3 \text{ mm}^3$  including the  
 147 reflector part, and half of all the scintillator bars have 5-cm-interval slits to form the grid  
 148 structure (Figure 6 ).

149 We will have two types of the Wagasci modules, a water-in module and a water-out  
 150 module. The water-in Wagasci module has water in spaces of the grid structure. The total  
 151 water mass serving as neutrino targets in the fiducial volume of the module is 188 kg, and  
 152 the mass ratio of scintillator bars to water is 80 %. The water-out Wagasci module doesn't  
 153 have water inside the detector. The total CH mass serving as neutrino target in the fiducial  
 154 volume of the module is 47 kg, and the mass fraction of scintillator bars is 100 %.

155 Scintillation light is collected by wave length shifting fibers, Y-11 (non-S type with a  
 156 diameter of 1.0 mm produced by Kuraray. A fiber is glued by optical cement in a groove  
 157 on surface of a scintillator bar. 32 fibers are gathered together by a fiber bundle at edge

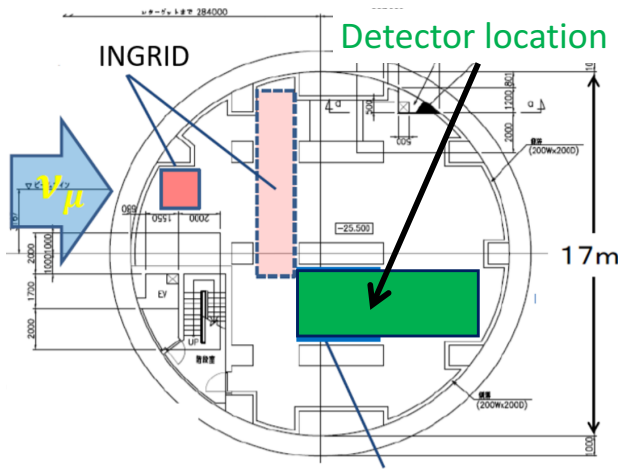


Figure 3: Candidate detector position in the B2 floor of the near detector hall.

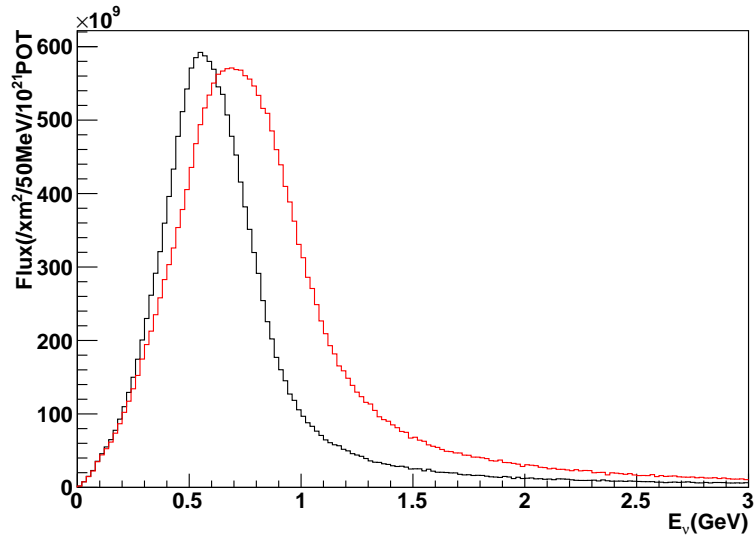


Figure 4: Neutrino energy spectrum at the candidate detector position(red, off-axis 1.5 degree). The spectrum at the ND280 site (black, off-axis 2.5 degree) is also shown.

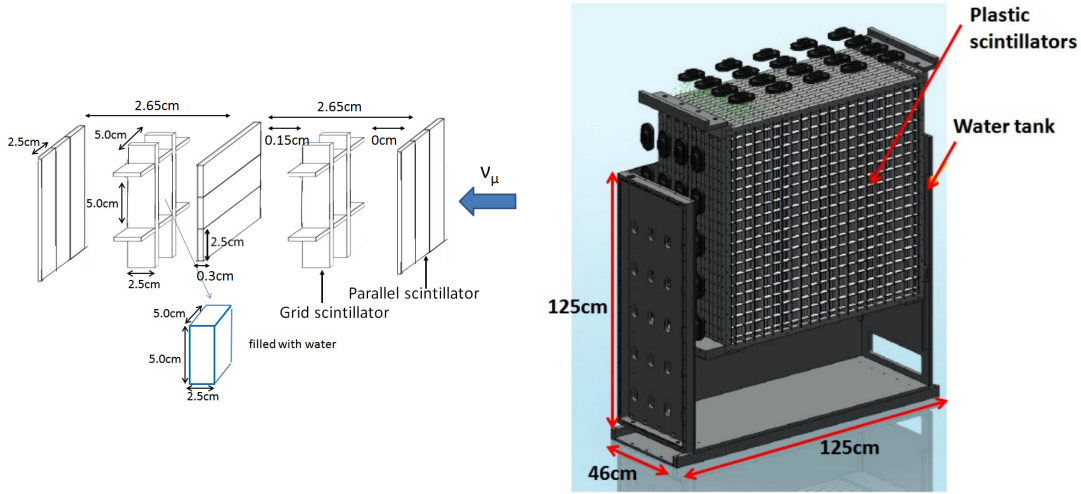


Figure 5: Schematic views of 3D grid-like structure of plastic scintillator bars (left) and Wagasci module (right).

of the module, and lead scintillation light to a 32-channel arrayed MPPC. Since crosstalk of light yield due to reflection on the inner surface of each cell has been observed, all the scintillator bars are painted black by aqueous color spray. It is confirmed by measurements with cosmic rays that black painting on the surface of the scintillator bars suppresses this crosstalk so that no significant crosstalk effect is observed within uncertainty.

32-channel arrayed MPPCs, as shown in the Fig. 7, are used for the modules. The surface of the fiber bundle is polished and directly attached onto the 32-channel arrayed MPPCs. The positions of 32 fibers on the bundle are aligned to fit the channels of MPPCs. The MPPC is a product of Hamamatsu Photonics, S13660(ES1), with suppressed noise rate of  $\sim 6$  kHz per channel at 0.5 p.e. threshold. For each MPPC channel, 716 pixels of APD are aligned in a shape of circle.

### 2.1.2 Electronics

As front-end electronics of this detector, a Silicon PM Integrated Read-Out Chip (SPIROC) [12] is adopted. SPIROC is a 36-channel auto-triggered front-end ASIC, and is produced by OMEGA/ IN2P3. It not only contains an analog signal processing part such as amplification and shaping of the waveform, but contains a digital signal processing parts such as auto-trigger and timing measurement. Charge of MPPC signal is sampled by track-and-hold circuit. A Front-end electronics board, Active Sensor Unit (ASU), has been developed with the SPIROC2D chip, which is the latest version of SPIROC. Each readout board is designed to control a 32-channel arrayed MPPC, and 40 of the ASU boards are aligned on

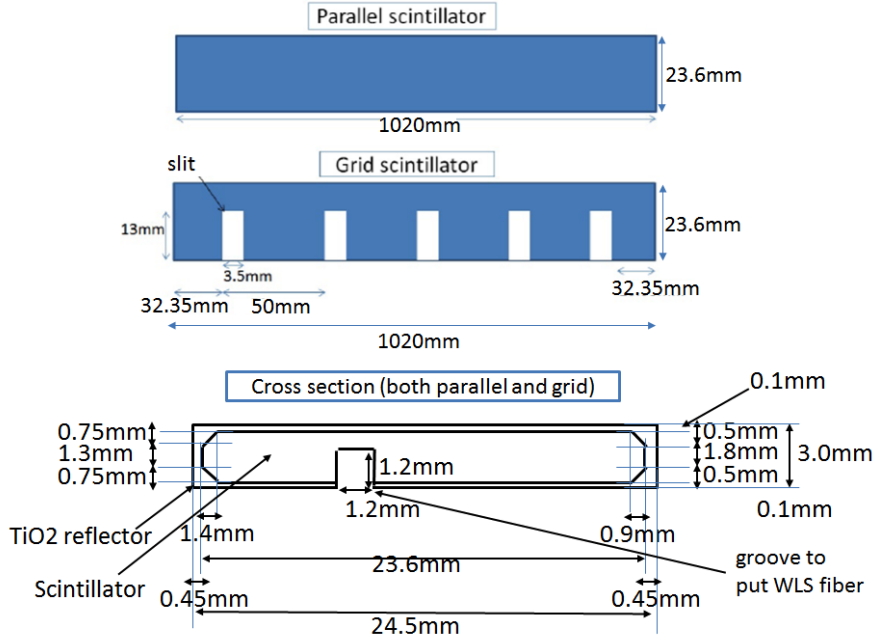


Figure 6: Geometry of scintillators used for Wagasci modules.

178 the module surface. The data acquisition system used for this detector, including back-end  
 179 boards, has been developed for prototypes of ultra-granular calorimeters for the Interna-  
 180 tional Linear Collider (ILC) [5], and independent of the T2K DAQ system. To synchronize  
 181 the DAQ system to J- PARC neutrino beam, pre-beam trigger and beam trigger are sent to  
 182 the clock control card. The beam trigger signals are converted from optical signals to NIM  
 183 signals at NIM module on the B2 floor. In addition, the information of spill number are  
 184 delivered with 16-bit ECL level signals, and converted to an Ethernet frame by an FPGA  
 185 evaluation board to be directly sent to the DAQ PC. The electronics readout scheme is  
 186 shown in Fig. 8.

187 **2.1.3 Water system**

188 Pure water is filled to the water tank of the water-in Wagasci module as follows. First,  
 189 the water storage tank located at the B2 floor of the NM pit is filled with water delivered  
 190 from a water tap on the ground level through a long hose. Second, the water is pumped  
 191 to the other water storage tank though a water filler to produce pure water. Third, a  
 192 compound preservative called Germall plus, which is the same preservative used in one of  
 193 the sub-detectors of T2K ND280, FGD2, is put into the water to keep water from being  
 194 bad. Then, the water is poured to the water-in Wagasci module, and it is kept in the

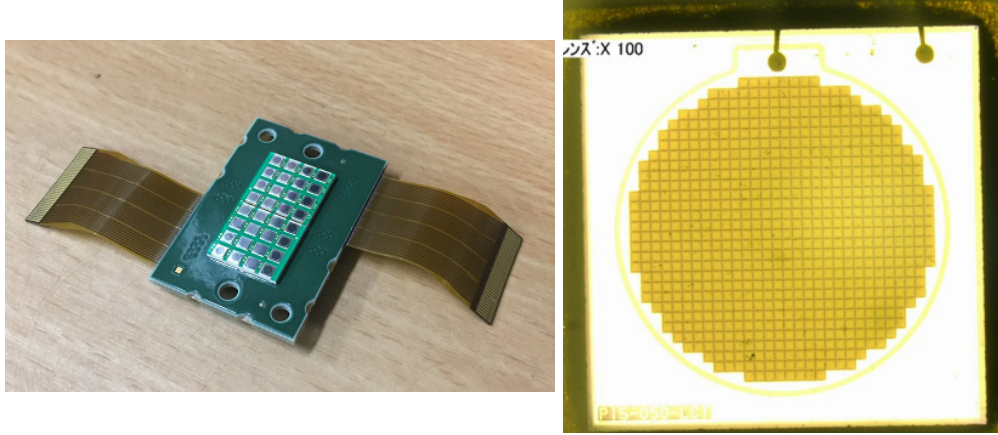


Figure 7: 32-channel arrayed MPPC (left) and an enlarged view of one MPPC channel (right).

195 module during the neutrino beam operation and not to be circulated.

## 196 2.2 INGRID Proton module

197 INGRID Proton module is a neutrino detectors of the T2K experiment. It is a fully-active  
198 tracking detector which consists of only scintillator strips. The purpose of this Proton  
199 Module is to separate the neutrino interaction types by detecting the protons and pions  
200 together with the muons from the neutrino interactions, and to measure the neutrino cross  
201 section for each interaction type. It consists of 36 tracking planes surrounded by veto planes  
202 (Figure 9), where each tracking plane is an array of two types of scintillator strips. The  
203 16 strips in the inner region have dimensions of  $2.5\text{cm} \times 1.3\text{cm} \times 120\text{cm}$ , while the 16 strips  
204 in the outer region have dimensions of  $5\text{cm} \times 1\text{cm} \times 120\text{cm}$ , making a plane of  $120 \times 120\text{cm}^2$   
205 in the horizontal and vertical directions. The former is the scintillator produced for the  
206 K2K SciBar detector [3] and the latter was produced for INGRID. The tracking planes are  
207 placed perpendicular to the beam axis at 23mm intervals. Since the strips are aligned in one  
208 direction, each tracking plane is sensitive to either the horizontal or vertical position of the  
209 tracks. The tracking planes are therefore placed alternating in the horizontal and vertical  
210 directions so that three-dimensional tracks can be reconstructed. The tracking planes also  
211 serve as the neutrino interaction target. As with the Wagasci modules, scintillation light  
212 is read out by a WLS fiber and MPPC.

213 It was installed at the neutrino beam axis on the SS floor of the T2K near detector hall  
214 in 2010, and had been used for neutrino cross section measurements. In August 2017, it  
215 was moved to the B2 floor of the T2K near detector hall by J-PARC T59 after getting the  
216 approval from T2K to use them. J-PARC T59 is performing a neutrino beam measurement

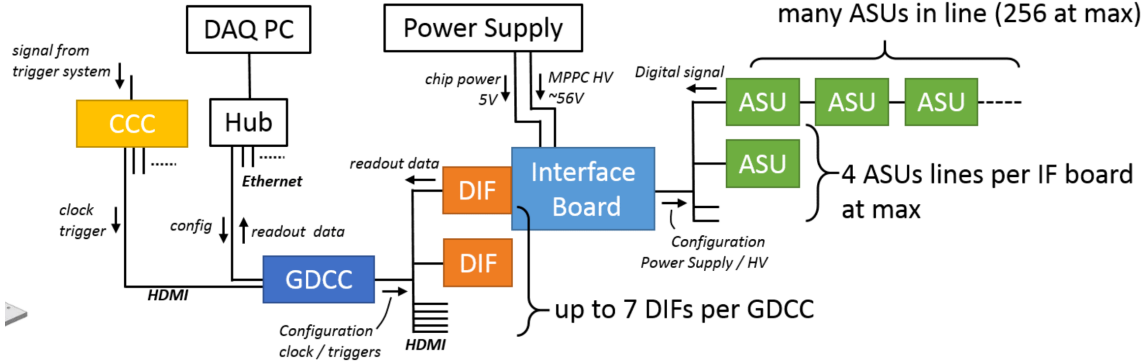


Figure 8: Wagasci electronics readout scheme.

217 using the detector from October 2017, and the measurement will continue until May 2018  
 218 as we will discuss in Sec. 4.

219 We will operate the INGRID Proton module using the T2K near detector electronics/  
 220 DAQ system in the same way as J-PARC T59. A proposal to use the module and its  
 221 electronics for our project will be submitted to the T2K collaboration.

### 222 2.3 Baby MIND

223 The Baby MIND is the downstream Muon Range Detector. It also works as a magnet and  
 224 provides the charge identification capability as well as magnetic momentum measurement  
 225 for high energy muons.

226 The Baby MIND collaboration <sup>1</sup> submitted a proposal to the SPSC at CERN, SPSC-P-  
 227 353. The project was approved by the CERN research board as Neutrino Platform project  
 228 NP05 and constructed. The detector consists of 33 magnet modules, each 3500 mm ×  
 229 2000 mm × 50 mm (30 mm steel) with a mass of approximately 2 tonnes. Of these magnet  
 230 modules, 18 are instrumented with plastic scintillator modules.

#### 231 2.3.1 Magnet modules

232 The Baby MIND is built from sheets of iron interleaved with scintillator detector modules  
 233 but unlike traditional layouts for magnetized iron neutrino detectors (e.g. MINOS) which  
 234 tend to be monolithic blocks with a unique pitch between consecutive steel segments and  
 235 large conductor coils threaded around the whole magnet volume, the Baby MIND iron  
 236 segments are all individually magnetized as shown in Fig. 10, allowing for far greater  
 237 flexibility in the setting of the pitch between segments, and in the allowable geometries  
 238 that these detectors can take.

---

<sup>1</sup>Contact person: E. Noah, Spokesperson: A. Blondel, Deputy spokesperson: Y. Kudenko

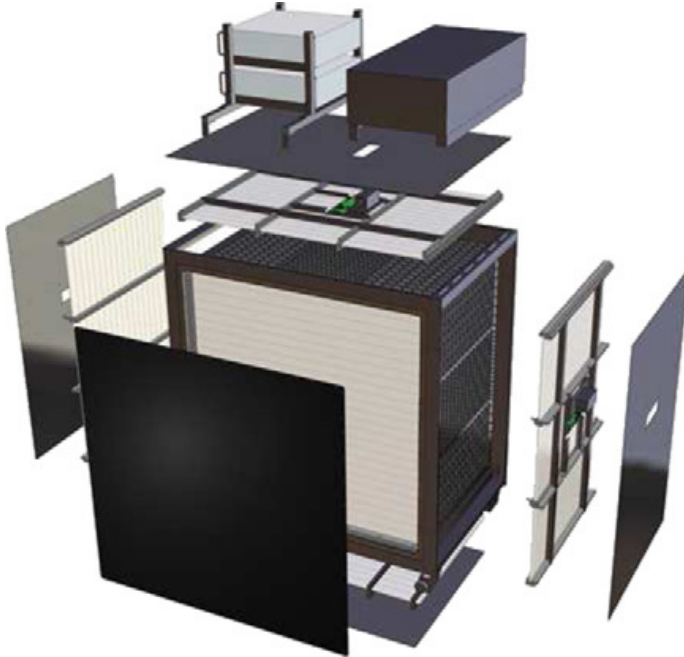


Figure 9: Schematic view of INGRID Proton module.

239        The key design outcome is a highly optimized magnetic field map. A double-slit con-  
 240        figuration for coil winding was adopted to increase the area over which the magnetic flux  
 241        lines are homogeneous in  $B_x$  across the central tracking region. Simulations show the  
 242        magnet field map to be very uniform over this central tracking region covering an area of  
 243         $2800 \times 2000 \text{ mm}^2$ , Fig. 11. The  $B_x$  component dominates in this region, with negligible  
 244         $B_y$  and  $B_z$ . This was confirmed by measuring the field with 9 pick-up coils wound around  
 245        the first module. Subsequent modules were equipped with one pick-up coil. Test results  
 246        on the 33 modules show all to achieve the required field of 1.5 T for a current of 140 A,  
 247        with a total power consumption of 11.5 kW. The polarity of the field map shown in Fig. 11  
 248        (middle) can be reversed by changing the power supply configuration.

249        **2.3.2 Scintillator modules**

250        Each of the 18 scintillator modules is constructed from 2 planes of horizontal counters (95  
 251        counters in total) and 2 planes of vertical counters (16 counters in total) [2], arranged  
 252        with an overlap between planes to achieve close to 100% hit efficiency for minimum ioniz-  
 253        ing muons. The arrangement of planes within a module is vertical-horizontal-horizontal-  
 254        vertical. This arrangement was the result of an assembly approach whereby each plane  
 255        was built from 2 half-planes, with each half plane consisting of a horizontal plane and a

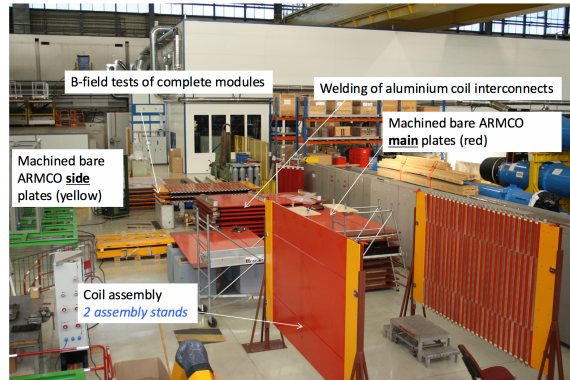


Figure 10: Magnet assembly zone at CERN.

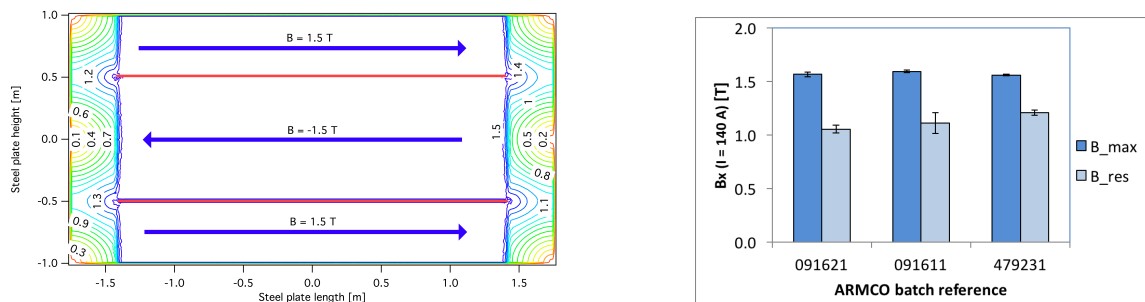


Figure 11: Left) Magnetic field map with a coil along 280 cm of the length of the plate. Right) Measured B field for 33 modules.

256 vertical plane. The scintillator bars are held in place using structural ladders that align  
257 and maintain the counters, Fig. 12. No glue is used in the process, so counters can be  
258 replaced. Aluminum sheets front and back provide light tightness.



Figure 12: Scintillator modules assembly. Left) top of front half-module showing vertical counters, and the spacers-ladders that set the pitch between horizontal counters and hold them in place. Middle) rear half-module showing horizontal counters on their ladders. Right) Assembled rear half-module, the front half-module can be seen in the background.

259 The plastic scintillator counters were made from 220 mm-wide slabs, consisting of  
260 extruded polystyrene doped with 1.5% paraterphenyl (PTP) and 0.01% POPOP. They were  
261 cut to size then covered with a 30-100  $\mu\text{m}$  thick diffuse reflector resulting from etching of  
262 the surface with a chemical agent [9, 10]. The horizontal counter size is  $2880 \times 31 \times 7.5 \text{ mm}^3$ ,  
263 with one groove along the length of the bar in which sits a wavelength shifting fiber from  
264 Kuraray. The vertical counter size is  $1950 \times 210 \times 7.5 \text{ mm}^3$ , with one U-shaped groove  
265 along the bar. On each counter, two custom connectors house silicon photomultipliers,  
266 MPPC type S12571-025C from Hamamatsu, either side of the horizontal counter, and  
267 both connectors at the top for the vertical counter. This geometrical configuration for  
268 vertical counters was chosen for ease of connectivity to the electronics, and maintenance  
269 operations.

270 A total of 1744 horizontal counters and 315 vertical counters (including spares) were  
271 produced at the Uniplast company (Vladimir, Russia).

### 272 **2.3.3 Electronics**

273 The Baby MIND electronic readout scheme includes several custom-designed boards [11].  
274 The revised version is shown in Fig. 13. At the heart of the system is the electronics  
275 Front End Board (FEB), developed by the University of Geneva. The readout system  
276 includes two ancillary boards, the Backplane, and the Master Clock Board (MCB) whose  
277 development has been managed by INRNE (Bulgarian Academy of Sciences) collaborators.

278 The FEBv2 hosts 3 CITIROC chips that can each read in signals from 32 SiPMs [6].  
279 Each signal input is processed by a high gain, and a separate low gain, signal path. The  
280 outputs from the slow shapers can be sampled using one of two modes: a mode with an  
281 externally applied delay, and a peak detector mode. A faster shaper can be switched to

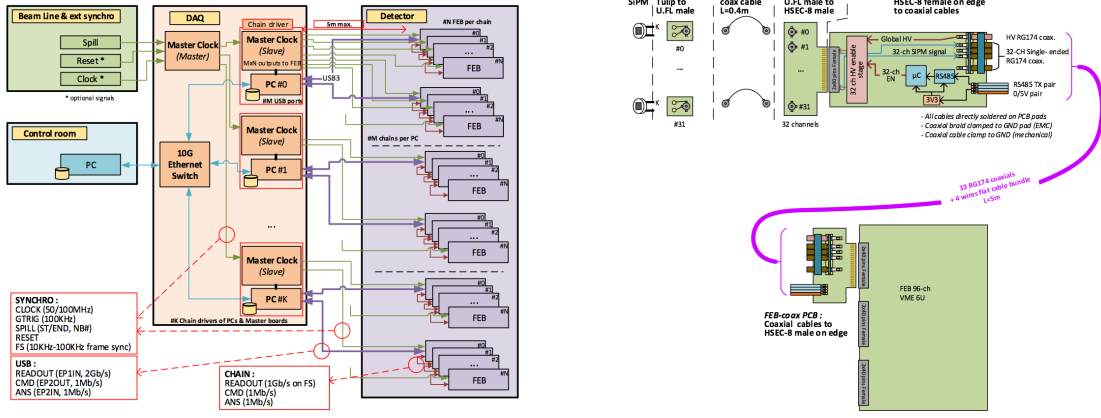


Figure 13: Left) Baby MIND electronics readout scheme. Right) SiPM-to-FEB connectivity.

either HG or LG paths, followed by discriminators with adjustable thresholds providing 32 individual trigger outputs and one OR32 trigger output. An Altera ARIA5 FPGA on the FEBv2 samples these trigger outputs at 400 MHz, recording rising and falling times for the individual triggers and assigning time stamps to these. Time-over-threshold from the difference between falling and rising times gives some measure of signal amplitude, used in addition to charge information and useful if there is more than one hit per bar within the deadtime due to the readout of the multiplexed charge output of  $\sim 9 \mu\text{s}$ . The ARIA5 also manages the digitization of the sampled CITIROC multiplexed HG and LG outputs via a 12-bit 8-ch ADC.

The internal 400 MHz clock on the FEBv2 can be synchronized to a common 100 MHz clock. The synchronization subsystem combines input signals from the beam line into a digital synchronization signal (SYNC) and produces a common detector clock (CLK) which can eventually be synchronised to an external experiment clock. Both SYNC and CLK signals are distributed to the FEBs. Tests show the FEB-to-FEB CLK(SYNC) delay difference to be 50 ps (70 ps). Signals from the beam line at WAGASCI include two separate timing signals, arriving 100 ms and 30  $\mu\text{s}$  before the neutrino beam at the near detectors. The spill number is available as a 16-bit signal.

### 2.3.4 Pefromance check

All counters were measured at INR Moscow with a cosmic ray setup using the same type S12571-025C MPPCs and CAEN DT5742 digitizer. The average light yield (sum from both ends) was measured to be 37.5 photo-electrons (p.e.) per minimum ionizing particle (MIP) and 65 p.e./MIP for vertical and horizontal counters, respectively. After shipment to CERN, all counters were tested once more individually with an LED test setup [?]. 0.1% of

305 counters failed the LED tests and were therefore not used during the assembly of modules.  
 306 The assembly of modules was completed in June 2017, and it was then tested in June and  
 307 July 2017 at the Proton Synchrotron experimental hall at CERN with a mixed particle  
 308 beam comprising mostly muons whose momenta could be selected between 0.5 and 5 GeV/c.  
 An event display from the summer 2017 tests is shown in Fig. 14.

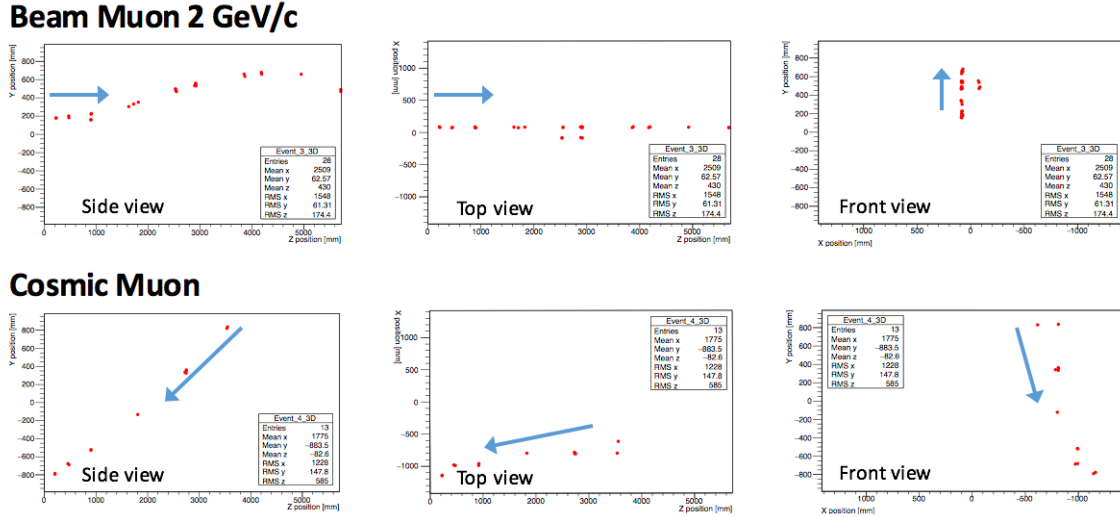


Figure 14: Comparison of a beam muon and cosmic muon in the three different geometrical projections of the detector. The beam impinges on the detector from the left. The arrows indicate the direction of travel of these muons. The direction of the cosmic muon is inferred from timing information.

309

## 310 2.4 Side muon range detector

311 Two Side-MRD modules for tracking secondary particles from neutrino interactions will be  
 312 installed in 2018. Each Side-MRD module is composed of 11 steel plates and 10 layers of  
 313 total 80 scintillator slabs installed in 13 mm gaps between the 30 mm thick plates. Each  
 314 steel plate size is  $30 \times 1610 \times 1800$  mm $^3$ . Total module size is  $2236 \times 1630 \times 975$  mm $^3$  as  
 315 shown in Fig. 15 (left), weight is  $\sim 8.5$  ton.

316 Scintillator bars were manufactured by Uniplast company in Vladimir, Russia. Polystyrene  
 317 based scintillators were extruded with thickness of 7 mm, then cut to the size of  $7 \times 200 \times$   
 318  $1800$  mm $^3$ . Dopant composition is 1.5% PTP and 0.01% POPOP. Scintillator surface was  
 319 etched by a chemical agent to form a white diffuse layer with excellent reflective perfor-  
 320 mance. Ideal contact between the scintillator and the reflector raises the light yield up to  
 321 50% comparing to an uncovered scintillator. Sine like groove was milled along the scin-  
 322 tillator to provide uniform light collection over the whole scintillator surface. WLS Y11

323 Kuraray fiber of 1 mm diameter is glued with an optical cement EJ-500 in the S-shape  
 324 groove as shown in Fig. 15(right). Bending radius is fixed to 30 mm that was specified to  
 325 be safe for Kuraray S-type fibers. Both ends of the fiber are glued into optical connectors  
 326 which mounted within a scintillator body and provide an interface to SiPMs, Hamamatsu  
 327 MPPC S13081-050CS(X1).

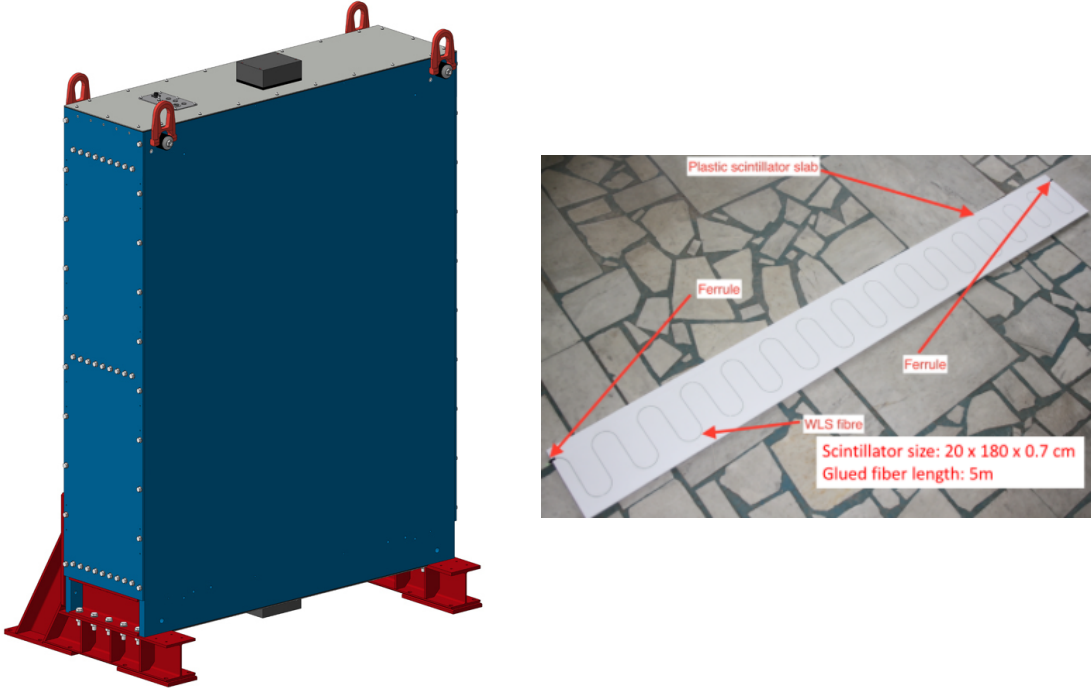


Figure 15: Left :Side-MRD module. Right: Scintillator bar of the Side-MRD modules.

328 Scintillators for the Side-MRD modules had been assembled at INR in Russia, and  
 329 shipped to Japan in July 2017. The light yield for each scintillator was measured with  
 330 cosmic rays at INR and at YNU in Japan after delivery. Parameters measured at the  
 331 center of the counter were : the light yields  $LY_1$  and  $LY_2$  at both ends, the light yield  
 332 asymmetry between the ends calculated as  $100\% \times \frac{LY_1 - LY_2}{LY_1 + LY_2}$ . After tests at INR we selected  
 333 324 counters from measured 332 ones with the mean light yield of 45 p.e./MIP (  $LY_1 + LY_2$   
 334 ) and the asymmetry value less than 10 % . The measuremens at YNU yielded the average  
 335 total light yield of about 40 p.e./MIP which varies in range from 32 to 50 p.e./MIP (Fig.  
 336 16 (left)). Only two counters showed relatively high asymmetry close to 25 % as shown in  
 337 Fig. 16 (right). Using the results of the quality assurance test we selected 320 scintillator  
 338 counters for the Side-MRD modules.

339 We also measured the time resolution for a combination of four counters piled each on  
 340 another one. The average result for four counters is  $\sigma_T = 1.04$  ns. The resolution of com-  
 341 bination of 2, 3, 4 counters is measured to be 0.79 ns, 0.66 ns and 0.58 ns, correspondently.

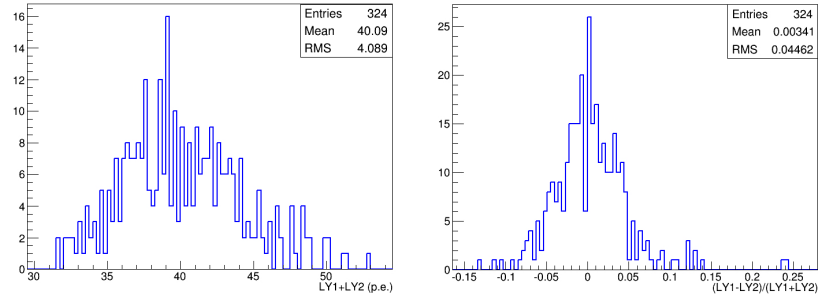


Figure 16: Total light yield distribution (left) and light yield assymetry (right) measured at YNU.

342  
 343 Construction of Side-MRD modules will be done from November 2017 at Yokohama  
 344 National University, then they will be transported to J-PARC and will be installed at B2  
 345 floor of the T2K near detector hall.

346 Same electronics as the WAGASCI modules (see Sec. 2.1.2) are used for the Side-MRD  
 347 modules.

### 348 3 Physics goals

349 We will measure the differential cross section for the charged current interaction on H<sub>2</sub>O  
 350 and Hydrocarbon(CH)). The water-scintillator mass ratio of the Wagasci module is as  
 351 high as 5:1 and the high purity measurement of the cross section on H<sub>2</sub>O is possible. One  
 352 experimental option is to remove water from one of the two Wagasci modules. The water-  
 353 out WAGASCI module will allow to measure pure-CH target interactions with very low  
 354 momentum-threshold for protons. It will also benefit to subtract the background from  
 355 interaction with scintillator in the water target measurement. Another option is to add  
 356 the T2K proton module which is fully made of plastic scintillators. It will allow the high  
 357 statistics comparison of cross section between H<sub>2</sub>O and CH and also comparison with  
 358 the ND280 measurement. The actual configuration will be optimized with detailed MC  
 359 simulation by 2018 Summer.

360 Our setup allows the measurements of inclusive and also exclusive channels such as 1- $\mu$ ,  
 361 1- $\mu 1p$ , 1- $\mu 1\pi \pm np$  samples, former two of which are mainly caused by the quasi-elastic and  
 362 2p2h interaction and the latter is mainly caused by resonant or coherent pion production

and deep elastic scattering. In general, an accelerator produced neutrino beam spectrum is wide and the energy reconstruction somehow rely on the neutrino interaction model. Therefore, recent neutrino cross section measurement results including those from T2K are given as a flux-integrated cross section rather than cross sections as a function of the neutrino energy to avoid the model dependency. We can provide the flux-averaged cross section. In addition, by combining our measurements with those at ND280, model-independent extraction of the cross section for narrow energy region becomes possible. This method was demonstrated in [1] and also proposed by P\*\* (NUPRISM).

### 3.1 Expected number of events

Expected number of neutrino events after the event selections is evaluated with Monte Carlo simulations as we will discuss in Section 5. In the neutrino-mode,  $4.2 \times 10^3$ ,  $1.1 \times 10^3$  and  $3.8 \times 10^3$  CC neutrino events are expected in the water-in WAGASCI module, the water-out WAGASCI module and the INGRID proton module after the selections with  $0.5 \times 10^{21}$  POT, and its purities are 78.0 %, 97.5 % and  $\sim 98\%$ . In the antineutrino-mode,  $1.7 \times 10^3$ ,  $0.4 \times 10^3$  and  $1.5 \times 10^3$  CC antineutrino events are expected in the water-in WAGASCI module, the water-out WAGASCI module and the INGRID proton module after the selections with  $0.5 \times 10^{21}$  POT, and its purities are 59.5 %, 74.4 % and  $\sim 74\%$ .

Statistical errors of flux integrated CC-inclusive neutrino cross section measurements on H<sub>2</sub>O (full acceptance) and CH targets (forward acceptance) will be 1.5 % and 1.6 % with  $0.5 \times 10^{21}$  POT in the neutrino-mode. Statistical errors of flux integrated CC-inclusive antineutrino cross section measurements on H<sub>2</sub>O (full acceptance) and CH targets (forward acceptance) will be 2.4 % and 2.5 % with  $0.5 \times 10^{21}$  POT in the antineutrino-mode.

Statistical errors of flux integrated H<sub>2</sub>O to CH CC-inclusive neutrino cross section ratio measurement will be 3.1 % (full acceptance) and 2.3 % (forward acceptance) with  $0.5 \times 10^{21}$  POT in the neutrino-mode. Statistical errors of flux integrated H<sub>2</sub>O to CH CC-inclusive antineutrino cross section ratio measurement will be 5 % (full acceptance) and 3.7 % (forward acceptance) with  $0.5 \times 10^{21}$  POT in the antineutrino-mode.

### 3.2 Pseudo-monochromatic beam by using different off-axis fluxes

The off-axis method gives narrower neutrino spectrum, and the peak energy is lower for larger off-axis angle. There still remains high energy tail mainly due to neutrinos from Kaon decay. The off-axis angle of the Wagasci location is 1.5 degree and different from the ND280 2.5 degree. Top two plots of Fig. 17 show the energy spectra of fluxes and neutrino interaction events at these two different locations. The high energy tail of ND280 flux can be somehow subtraction by using the Wagasci measurement. The low energy part of the Wagasci flux can be also subtracted by using the ND280 measurement. Bottom two plots of Fig. 17 demonstrate this method. We can effectively get two fluxes, from 0.2 GeV to 0.9 GeV and 0.6 GeV and 2 GeV and measure flux-integrated cross section for these two

400 fluxes.

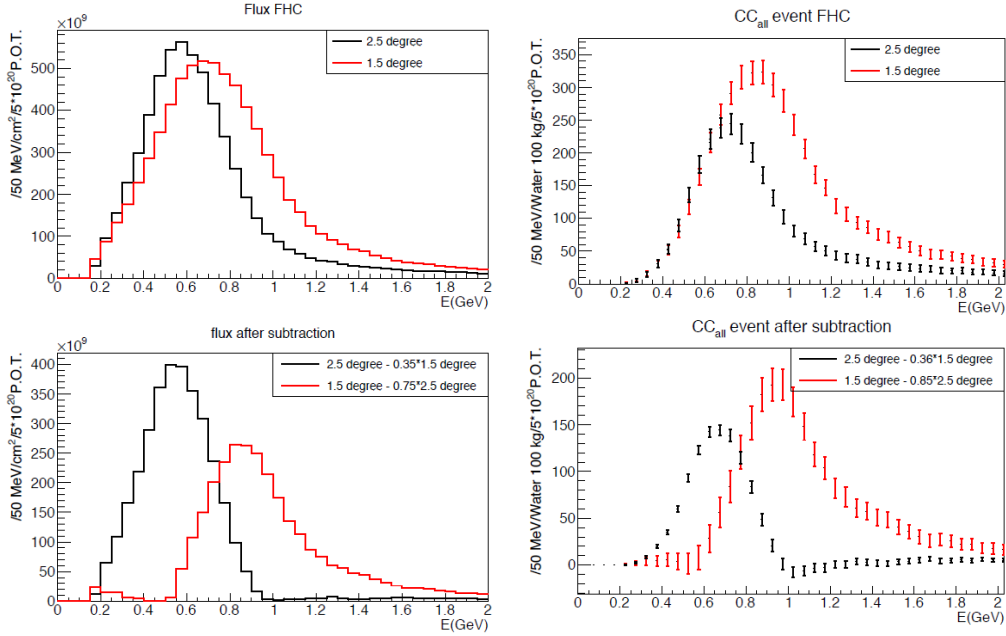


Figure 17: Energy spectra obtained by using different off-axis angle fluxes. Top two plots show the fluxes(left) and spectra of interaction events (right) for ND280 (off-axis 2.5 degree) and Wagasci (off-axis 1.5 degree). Bottom two plots show the fluxes (left) and spectra of interaction events (right) obtained by subtraction of fluxes at ND280 and Wagasci. The error bar is for the statistical error and those in the bottom right plot is obtained assuming the statistical error for ND280 measurement is much smaller than that of Wagasci experiment.

401 Statical errors of flux integrated CC-inclusive neutrino cross section measurements  
 402 on H<sub>2</sub>O (forward acceptance) and CH targets (forward acceptance) with the pseudo-  
 403 monochromatic beam will be 2 % and 1.9 % with  $0.5 \times 10^{21}$  POT in the neutrino-mode.  
 404 Statical errors of flux integrated CC-inclusive antineutrino cross section measurements  
 405 on H<sub>2</sub>O (forward acceptance) and CH targets (forward acceptance) with the pseudo-  
 406 monochromatic beam will be 3 % and 2.8 % with  $0.5 \times 10^{21}$  POT in the neutrino-mode.

### 407 3.3 Subjects Wagasci can contribute

408 In T2K experiment, neutrinos interact with bound nucleons in relatively heavy nuclei  
 409 (Carbon and Oxygen), so the cross-section is largely affected by nuclear effects. The nuclear  
 410 effects are categorized as nucleons' momentum distribution in nucleus, interactions with

411 correlated pairs of nucleons in nucleus (two particles-two holes, 2p2h), collective nuclear  
412 effects and final state interactions (FSI) of secondary particles in the nuclei after the initial  
413 neutrino interactions.

414 The 2p2h interactions mainly happen through  $\Delta$  resonance interactions following a  
415 pion-less decay and interactions with a correlated nucleon pair. The 2p2h interactions are  
416 observed in electron scattering experiments [7] where the 2p2h events observed in the gap  
417 between Quasi-Elastic region and Pion-production region as shown in Fig. 18. Neutrino  
418 experiments also attempt to measure the 2p2h interactions, but separation of the QE peak  
419 and the 2p2h peak is more difficult because transferred momentum ( $p$ ) and energy ( $w$ )  
420 are largely affected by neutrino energies which cannot be determined event-by-event in the  
421 wide energy spectrum of the accelerator neutrino beam. Our model-independent narrow  
422 neutrino spectra extracted from combined analyses of our data and ND280 data are ideal  
423 for searching the 2p2h interaction because clearer separation of the QE peak and the 2p2h  
424 peak is expected. Another way to observe the 2p2h interaction is direct measurement of  
425 proton tracks in CC0 $\pi$  sample with low detection threshold and full acceptance. Fig. 19  
426 shows proton multiplicities after FSI in CCQE events and 2p2h events, and Fig. 20 shows  
427 opening angles among two proton tracks in the same samples. The water-out Wagasci  
428 can provide good sample for the 2p2h interaction search because its low density medium  
429 enables the detection of low momentum protons in addition to the full acceptance.

430 There are various models which describe the collective nuclear effects [8]. The  $Q^2$   
431 dependence of the effects can be tested by measuring angular distribution of muons in  
432 CC1- $\mu$  and CC1- $\mu 1p$  events. The uncertainties of the effects in low (high)  $Q^2$  regions can  
433 be constrained by observing the events with a forward-going (high-angle) muon, so it is  
434 essential to measure muon tracks with full acceptance.

435 T2K experiment is starting to use  $\nu_e$  CC1 $\pi$  events for its CP violation search to increase  
436 the statistics. One of the biggest uncertainty of the CC1 $\pi$  sample comes from the final  
437 state interactions of pions in the nuclei after the initial neutrino interactions because they  
438 change the multiplicity, charge and kinematics of the pions. The multi-pion production  
439 events can be migrated into the CC1 $\pi$  sample due to the FSIs, and they become important  
440 backgrounds. We can constrain the uncertainties from the pion FSIs by measuring pion  
441 rescattering in the detector and pion multiplicity in  $\nu_\mu$  CCn $\pi$  sample with low detection  
442 threshold and full acceptance for pion tracks. The water-out WAGASCI can provide good  
443 sample for the pion FSI studies because its low density medium enables the detection of  
444 low momentum pions in addition to the full acceptance.

## 445 4 Status of J-PARC T59 experiment

446 We had submitted a proposal of a test experiment to J-PARC in April 2014 to test a new  
447 detector with a water target, WAGASCI, at the neutrino monitor hall, and the proposal  
448 was approved as J-PARC T59. The project contains the side and downstream muon range

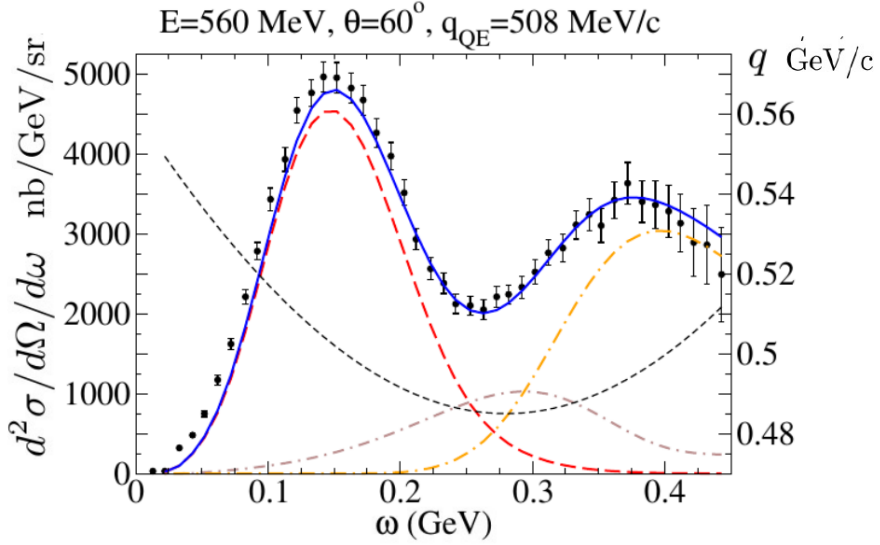


Figure 18: Comparison of inclusive  $^{12}\text{C}(\text{e},\text{e}')$  cross sections and predictions of the QE-SuSAv2 model (long-dashed red line), 2p-2h MEC model (dot-dashed brown line) and inelastic-SuSAv2 model (long dot-dashed orange line) (from Ref. [7]). The sum of the three contributions is represented with a solid blue line. The  $q$  dependence with  $w$  is also shown (short-dashed black line.)

detectors as well.

The first WAGASCI module has been constructed in 2016 and installed at the on-axis position in front of the T2K INGRID detector for the commissioning and the first cross section measurement as a part of the T2K experiment. The INGRID electronics boards are used to read the signal. The light yield measured with muons produced by the interaction of neutrinos in the hall wall, shown in Fig. 21, is sufficiently high to get good hit efficiency. A track search algorithm based on the cellular automaton has been developed using the software tools by the T2K INGRID. Examples of observed events are shown in Fig. 22. The tracking efficiency in 2-dimensional projected plane was evaluated by comparing the reconstructed track in the WAGASCI module and the INGRID module and shown in Fig. 23. Note that the tracking efficiency for high angle ( $> 70$  deg) is not evaluated because of the acceptance of the INGRID module, not because of the limitation of the WAGASCI module.

In 2017 Autumn, the construction of the second WAGASCI module and the dedicated electronics board were completed. The module and the electronics were installed to the B2 floor together with the T2K proton module and the INGRID module as shown in Fig. 24. The proton module is to be used as the entering muon veto and also for the comparison

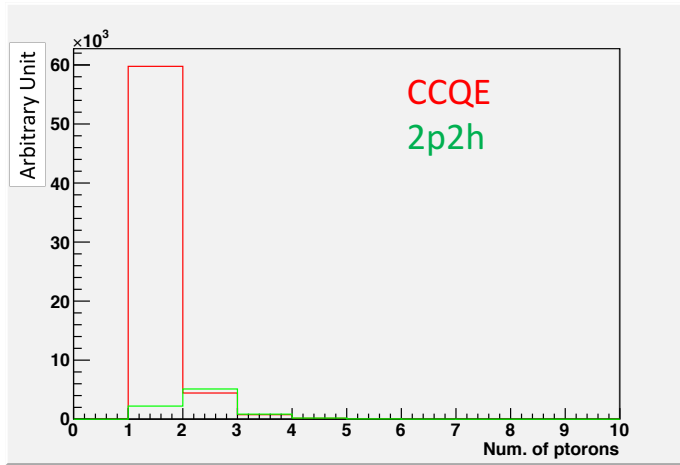


Figure 19: Proton multiplicities after FSI in CCQE events and 2p2h events.

466 of interaction between CH and Water. The INGRID module is for the temporary muon  
 467 detector with limited acceptance for this period. The detector was commissioned and is  
 468 in operation to take data with the antineutrino beam during the T2K beam time from  
 469 October.

470 The production of the components of the side muon range detectors has been completed  
 471 and now the detectors are being assembled at the Yokohama National University. These  
 472 detectors will be installed sometime from January to June, 2018 when T2K is not running.

473 The Baby MIND detector was transported from CERN to Japan in December, 2017.  
 474 It will be installed and commissioned in Jan.-Feb. 2018 and T59 will take the neutrino-  
 475 induced muon data in April and May.

## 476 5 MC studies

### 477 5.1 Detector simulation

478 Expected number of neutrino events in the water-in Wagasci detector is evaluated with  
 479 Monte Carlo simulations. Neutrino beam flux at the detector location is simulated by  
 480 T2K neutrino flux generator, JNUBEAM, neutrino interactions with target materials are  
 481 simulated by a neutrino interaction simulator, NEUT, detector responses are simulated  
 482 using GEANT4-based simulation. The neutrino flux at the detector location, 1.5 degrees  
 483 away from the J-PARC neutrino beam axis, is shown in Figure 4, and its mean neutrino  
 484 energy is around 0.68 GeV.

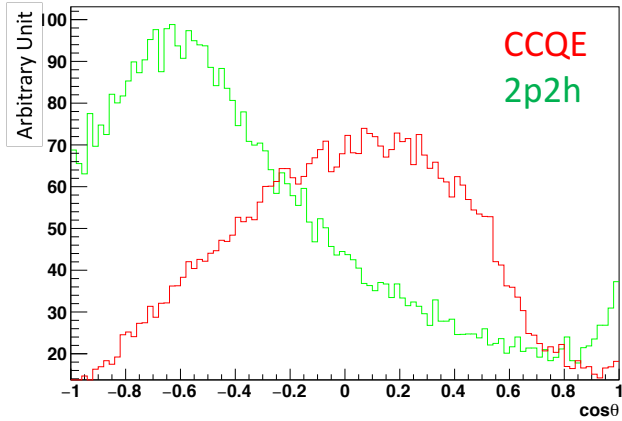


Figure 20: Opening angles among two proton tracks after FSI in CCQE events and 2p2h events.

#### 485 5.1.1 Detector geometry

486 The detector geometry in the GEANT4-based simulation is slightly different from the actual  
 487 detector as shown in Fig. 25. The active neutrino target region consists of four Wagasci  
 488 modules, and each Wagasci detector has the dimension with  $100\text{ cm} \times 100\text{ cm}$  in the x and  
 489 y directions and 50 cm along the beam direction. Two Side-MRD modules is installed at  
 490 both sides of the Wagasci modules, and each Side-MRD module consists of ten iron plates  
 491 whose dimension is 3 cm (thickness)  $\times$  200 cm (height)  $\times$  320 cm (width). The distance  
 492 between the Side-MRD modules and Wagasci modules is 80 cm. The downstream-MRD  
 493 equivalent to the Baby-MIND is installed at the downstream of the Wagasci modules. The  
 494 downstream-MRD consists of thirty iron plates whose dimension is 3 cm (thickness)  $\times$  200  
 495 cm (height)  $\times$  400 cm (width). The distance between the downstream-MRD modules and  
 496 Wagasci modules is 80 cm.

#### 497 5.1.2 Response of detector components

498 The energy deposit inside the scintillator is converted into the number of photons. The  
 499 effects of collection and attenuation of the light in the scintillator and the WLS fiber are  
 500 simulated, and the MPPC response is also taken into account. The light yield is smeared  
 501 according to statistical fluctuations and electrical noise.

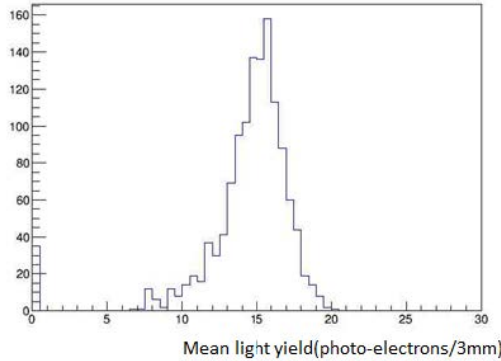


Figure 21: Light yield for muons produced by the interaction of neutrinos in the hall wall. Average light yields for each channel are plotted.

502    **5.2 Track reconstruction**

503    To select neutrino interaction from the hit patterns, a track reconstruction algorithm is  
504    developed. The flow of the track reconstruction is as follows.

505    1. Two-dimensional track reconstruction in each sub-detectors

506    2. Track matching among the sub-detectors

507    3. Three -dimensional track reconstruction

508    Add explanation about two-dim reco, track matching and three-dim reco here.

509    **5.3 Event selection**

510    First, the events with the track which starts in 5 cm from the wall of the Wagasci module  
511    are rejected to remove the background from the outside.

512    Second, to reject backgrounds from NC and neutral particles, the longest tracks are  
513    required to penetrate more than one (five) iron plates in Side-MRD modules (Baby-MIND).  
514    Then, in order to measure muon momentum, the longest tracks are required to stop in  
515    MRDs (Side-MRD modules and Baby-MIND) or penetrate all iron plates.

516    Table 1 and 2 show numbers of the selected events in one water-in Wagasci module  
517    after each event selection in neutrino-mode and antineutrino-mode respectively. As for  
518    the neutrino-mode, 8478 CC events are expected with  $1 \times 10^{21}$  POT, and the purity is  
519    78.0 %. The main background for the neutrino-mode is the neutrino interactions in the  
520    scintillators inside the Wagasci detector. As for the antineutrino-mode, 3331 CC events  
521    are expected with  $1 \times 10^{21}$  POT, and the purity is 59.5 %. The main background for the

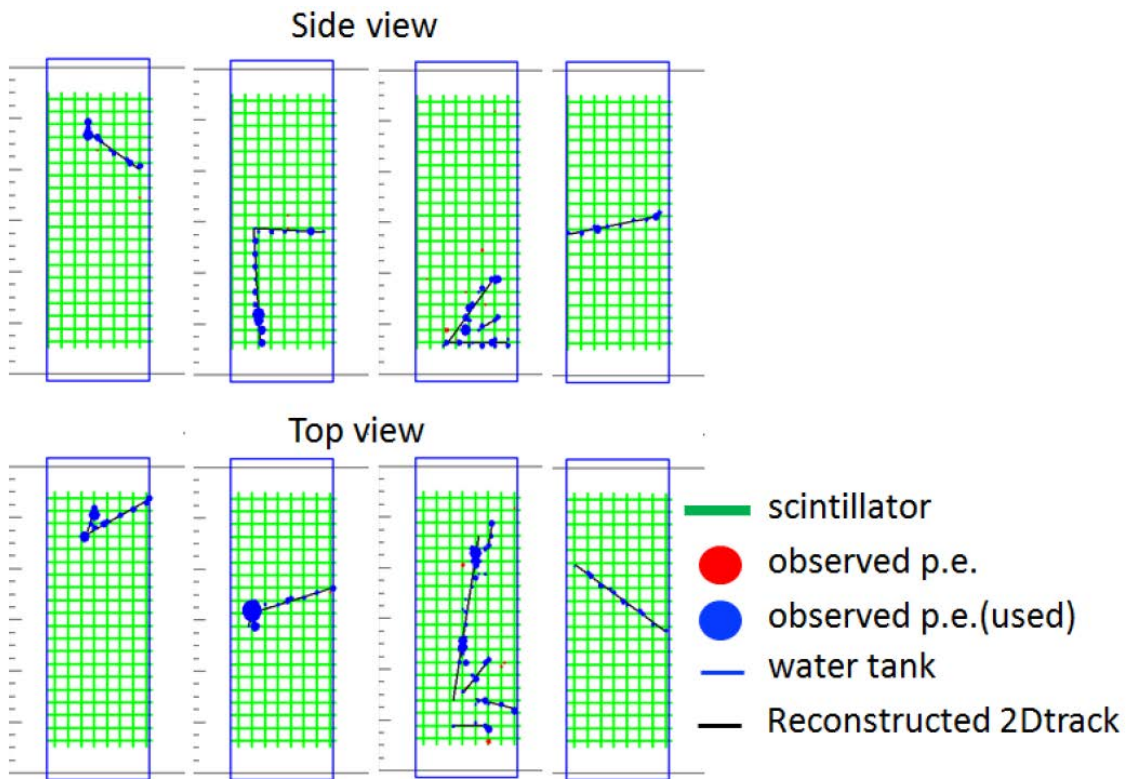


Figure 22: Example event displays of the WAGASCI module at on-axis. The reconstructed tracks are overlaid.

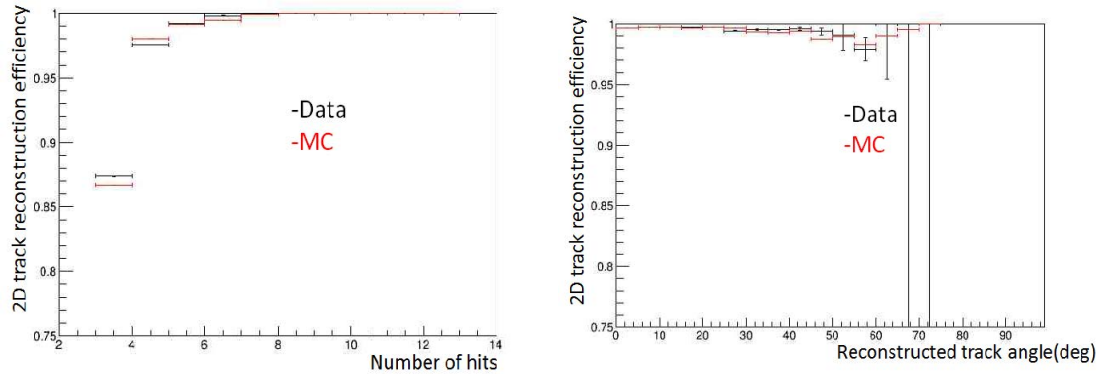


Figure 23: 2D track reconstruction efficiency as a function of number of hits (left) and track angle (right). Here the track angle is the one reconstructed by the INGRID module.

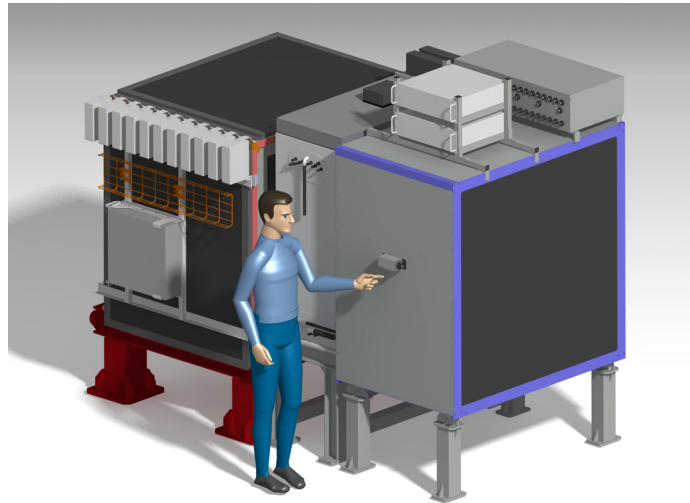


Figure 24: J-PARC T59 detector configuration in October 2017.

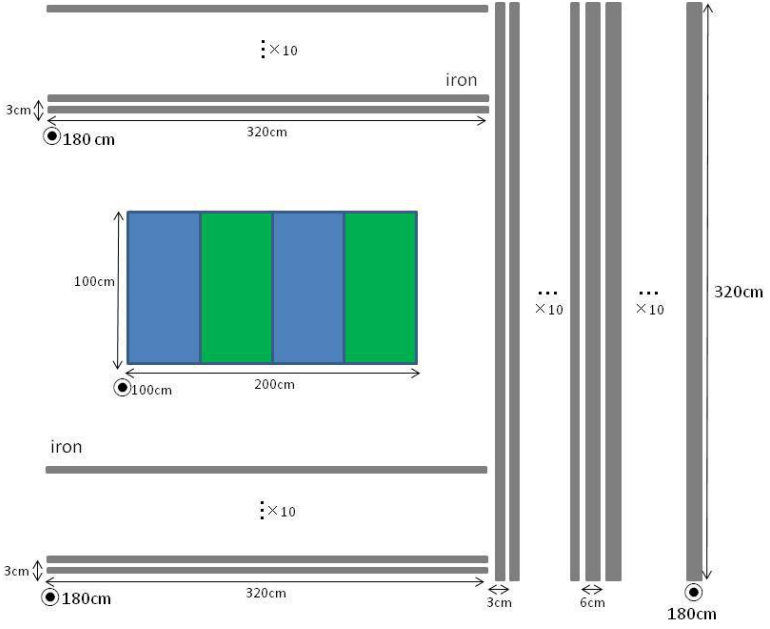


Figure 25: Geometry of the detectors in the Monte Carlo simulation.

antineutrino-mode is the wrong sign contamination from  $\nu_\mu$  events and the antineutrino interactions in the scintillators inside the Wagasci detector.

Table 3 and 4 show numbers of the charged-current events in the water-in Wagasci module after all event selection with a classification based on interactions at a vertex with  $1 \times 10^{21}$  POT in neutrino-mode and antineutrino-mode respectively.

Table 5 and 6 show numbers of the charged-current events in one water-in Wagasci module after all event selection with a classification based on particles after final state interactions with  $1 \times 10^{21}$  POT in neutrino-mode and antineutrino-mode respectively.

Figure 26 shows the reconstructed angles of the longest tracks in the selected events in the neutrino-mode and the anti-neutrino mode. Figure ?? shows the iron plane numbers in Side-MRD and Baby-MIND corresponding to the end points of the longest tracks in the selected events in the neutrino-mode and the anti-neutrino mode.

#### 5.4 Cross section measurements

The flux-averaged  $\nu_\mu$  ( $\bar{\nu}_\mu$ ) CC inclusive cross sections on water and hydrocarbon are calculated from the number of selected events using the background subtraction and efficiency

Table 1: Expected number of the neutrino-candidate events in one water-in Wagasci module with  $1 \times 10^{21}$  POT in neutrino-mode.

| Cut                 | CC      | NC    | Scinti Bkg. | Total   |
|---------------------|---------|-------|-------------|---------|
| Reconstructed       | 18093.2 | 699.7 | 4698.3      | 23491.2 |
| FV                  | 15150.8 | 588.4 | 3934.8      | 19673.9 |
| Pene. iron          | 11264.3 | 237.3 | 2875.4      | 14377.0 |
| Stop/Penetrate MRDs | 8478.2  | 214.0 | 2173.1      | 10865.2 |
| after all cuts      | 78.0 %  | 2.0 % | 20.0 %      | 100 %   |

Table 2: Expected number of the antineutrino-candidate events in one water-in Wagasci module with  $1 \times 10^{21}$  POT in antineutrino-mode.

| Cut                 | CC     | NC    | Scinti Bkg. | Wrong sign bkg | Total   |
|---------------------|--------|-------|-------------|----------------|---------|
| Reconstructed       | 6499.7 | 107.3 | 2234.4      | 2330.8         | 11172.1 |
| FV                  | 5457.9 | 89.3  | 1873.5      | 1946.6         | 9367.1  |
| Pene. iron          | 4172.3 | 30.8  | 1440.9      | 1560.6         | 7204.6  |
| Stop/Penetrate MRDs | 3331.5 | 28.5  | 1120.3      | 1121.2         | 5601.5  |
| after all cuts      | 59.5 % | 0.5 % | 20.0 %      | 20.0 %         | 100 %   |

537 correction

$$\sigma_{CC} = \frac{N_{sel} - N_{BG}}{\phi T \epsilon}, \quad (1)$$

538 where  $N_{sel}$  is the number of selected events from real data,  $N_{BG}$  is the number of selected  
 539 background events predicted by MC simulation,  $\phi$  is the integrated  $\nu_\mu$  flux,  $T$  is the number  
 540 of target nucleons, and  $\epsilon$  is the detection efficiency for CC events predicted by MC simula-  
 541 tion. in the water and hydrocarbon regions in the central detector. Finally, we will cancel  
 542 the dominant systematic error, the neutrino flux error, by comparing the cross-section re-  
 543 sults from two neutrino targets, water and hydrocarbon, having almost identical neutrino  
 544 fluxes, and measure the water to hydrocarbon charged current cross section ratio with 3%

Table 3: Expected number of the charged-current events in the water-in Wagasci module after the event selections with  $1 \times 10^{21}$  POT in neutrino-mode with a classification based on interactions at a vertex.

| CCQE   | MEC   | CCRes  | CCDIS  | Total  |
|--------|-------|--------|--------|--------|
| 3716.3 | 747.0 | 2081.3 | 1132.3 | 7676.9 |
| 48.4 % | 9.7 % | 27.1 % | 14.7 % | 100 %  |

Table 4: Expected number of the charged-current events in the water-in Wagasci module after the event selections with  $1 \times 10^{21}$  POT in antineutrino-mode with a classification based on interactions at a vertex.

| CCQE         | MEC   | CCRes  | CDDIS  | Total  |
|--------------|-------|--------|--------|--------|
| 2522.0       | 362.8 | 765.8  | 765.8  | 4416.4 |
| hline 57.1 % | 8.2 % | 17.3 % | 17.3 % | 100 %  |

Table 5: Expected number of the charged-current events in one water-in Wagasci module after the event selections with  $1 \times 10^{21}$  POT in neutrino-mode with a classification based on particles after final state interactions.

| CC0 $\pi$ | CC1 $\pi$ | CC2 $\pi$ | CCn $\pi$ | Total  |
|-----------|-----------|-----------|-----------|--------|
| 5423.1    | 1684.3    | 242.9     | 701.1     | 8051.4 |
| 67.4 %    | 20.9 %    | 3.0 %     | 8.7 %     | 100 %  |

precision, which is achieved in the INGRID measurement [4].

In the water target events, the background from interaction with scintillators has to be subtracted by using the measurement of the hydrocarbon target.

## 6 Standalone WAGASCI-module performances

In the previous sections, the WAGASCI detector was studied using the Muon Range Detectors. In this section, the standalone abilities of WAGASCI module are presented. Using the WAGASCI configuration presented in Section 5, we have evaluated that only 7% of the muons will be stopped in one of the WAGASCI modules. THower, this proportion increases to 53% for pions and 73% for protons produced by neutrino interactions at  $1.5^\circ$  off-axis. Figure 28 shows the momentum distribution of these daughter particles as well as for the sub-sample stopped in one of the WAGASCI modules. Therefore, the study of the

Table 6: Expected number of the charged-current events in one water-in Wagasci module after the event selections with  $1 \times 10^{21}$  POT in antineutrino-mode with a classification based on particles after final state interactions.

| CC0 $\pi$ | CC1 $\pi$ | CC2 $\pi$ | CCn $\pi$ | Total  |
|-----------|-----------|-----------|-----------|--------|
| 2529.3    | 520.0     | 37.9      | 96.0      | 3183.2 |
| 79.5 %    | 16.3 %    | 1.2 %     | 3.0 %     | 100 %  |

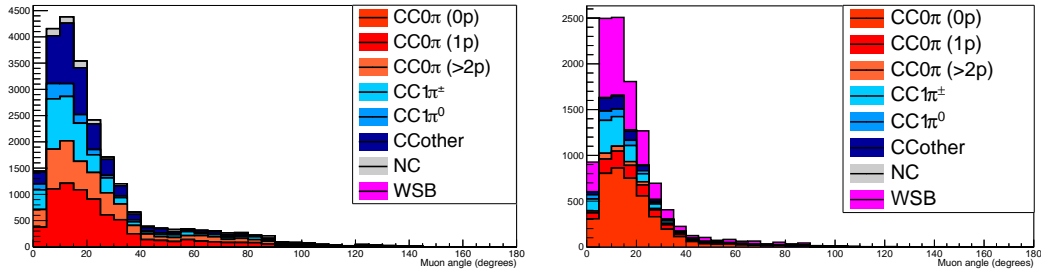


Figure 26: The reconstructed angles of the longest tracks in the selected events in the neutrino-mode (left) and the antineutrino-mode (right).

556 standalone abilities of the WAGASCI module in this section are dominantly motivated by:

- 557 • the accurate measurement of the neutrino interaction final states. Though most of the  
558 muons will be reconstructed and identified in the MRDs, the hadronic particles will  
559 predominantly stops in one WAGASCI module. One has therefore to rely exclusively  
560 on the WAGASCI module information alone to reconstruct, identify and measure the  
561 momentum of pions or protons.
- 562 • the coverage of the MRDs is not  $4\pi$ . Using the WAGASCI module information can  
563 therefore help to constraint the particles that exits the WAGASCI module but do  
564 not geometrically enters any MRD.
- 565 • the particle identification of low momenta muons  $p_\mu < 300 \text{ MeV}/c$  that will leave only  
566 few hits in the MRD. Using the WAGASCI module information will clearly enhance  
567 the particle identification.

568 This study is based on an original study done for the ND280 upgrade target, with some  
569 modifications. Though the cell size is similar to the WAGASCI configuration presented  
570 in Section 5, the external dimensions are different ( $186.4 \times 60 \times 130 \text{ cm}^3$ ). Whenever the  
571 results are presented with this external size and this parameter is likely to impact the  
572 result, it will be mentioned.

573 Note that in this section, a simplified reconstruction algorithm presented in Section 6.1 is  
574 used. The fiducial volume is chosen accordingly as the inner cube of the module which  
575 surfaces are distant of  $4 \times$  scintillator space = 10 cm from the module external surfaces.  
576 The neutrino interactions are simulated using NEUT v5.3.2. The NEUT input neutrino  
577 flux is estimated using JnuBeam v13a and assuming the detector to be located at  $1.5^\circ$   
578 off-axis, as in Section 5. Note that the event reconstruction efficiency as a function of true  
579 neutrino energy might be changed at  $1.5^\circ$ , due for example to different  $Q^2$  distributions. For  
580 this reason, one has to note that the reconstruction results might slightly be changed from

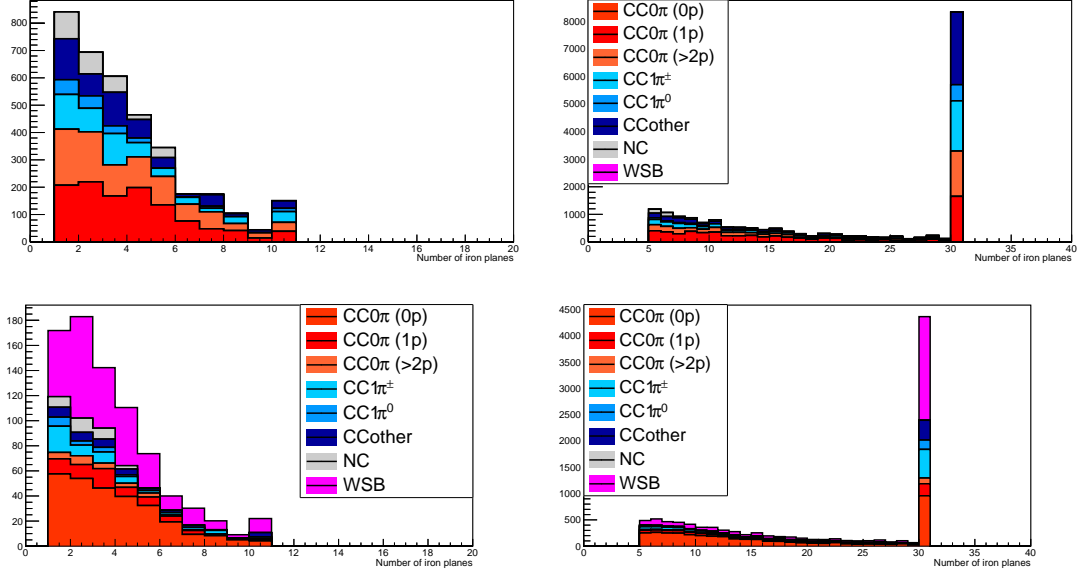


Figure 27: Iron plane numbers in Side-MRD (left) and Baby-MIND (right) corresponding to the end points of the longest tracks in the selected events in the neutrino-mode (top) and the antineutrino-mode (bottom).

581 2.5° and 1.5°. To avoid a similar change on the particle-only reconstruction efficiencies,  
 582 they will be presented as a function of variables that completely characterize the particle  
 583 kinematic state, *i.e.* its momentum and angle. Figure 29 shows the vertices distributions  
 584 of the daughter particles of neutrinos interacting one standard WAGASCI water-module.  
 585 In this section, we will show the detector reconstruction and particle identification in this  
 586 phase space, both for leptonic and hadronic particles. We will finally show an empty  
 587 WAGASCI module can highly enhance the ability to constrain the neutrino interaction  
 588 final state which is critical to reduce the corresponding uncertainties.

## 589 6.1 Reconstruction algorithm

### 590 6.1.1 Description

591 For this section, an ideal “simulated” reconstruction is developed. A particle is recon-  
 592 structed if:

- 593 1. The particle is charged.  
 594 2. Lets at least one hit (energy deposit > 2.5 photo-electron) in a scintillator.

595

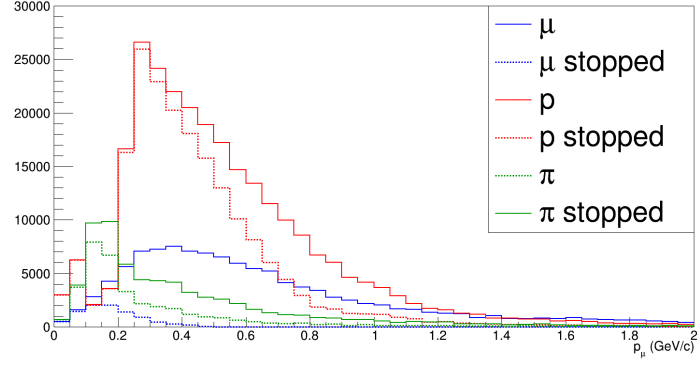


Figure 28: Momentum distribution of true particles in WAGASCI (plain) and corresponding distributions only for particles stopping into the WAGASCI module (dashed).

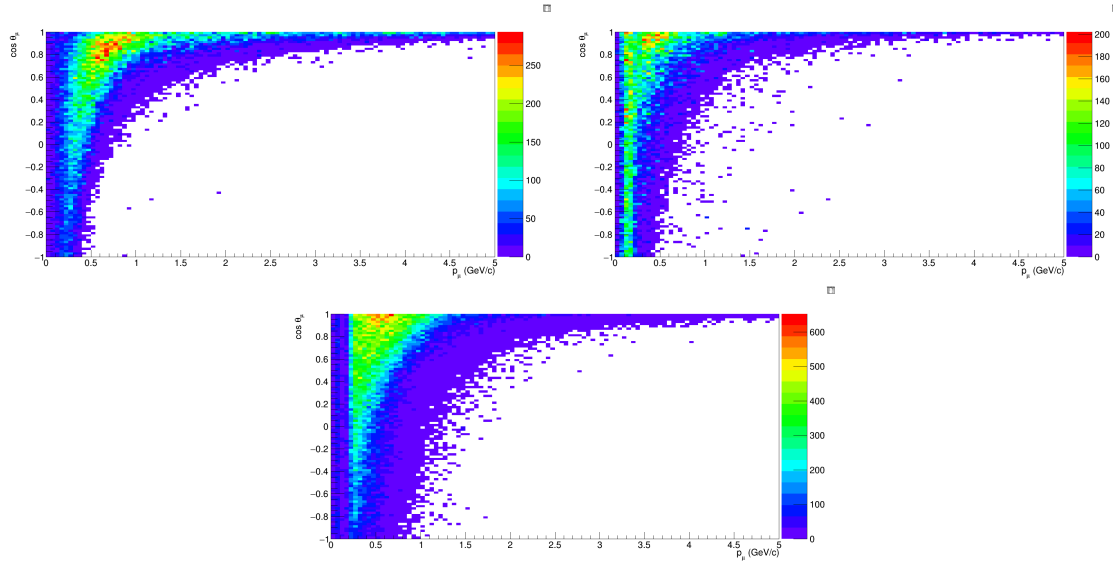


Figure 29: True number of muons (left), charged pions (right) and protons (bottom) in the two WAGASCI water-module as a function of the particles momenta and angles at  $1.5^\circ$ .

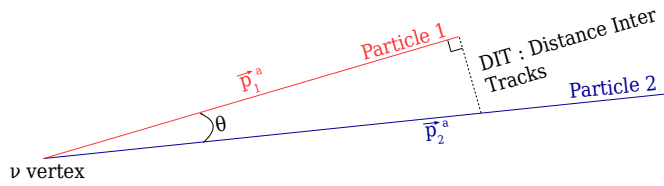


Figure 30: Definition of the distance inter tracks.

596        3. The particle enters one TPC and let one hit in the tracker.

597        Or

598

- 599        • The particle should be long enough to be reconstructed by the detector in at  
600        least 2 out of 3 views (XZ, YZ, XY). The length criterion requires the particle  
601        to let at least 4 hits in the detector. In the “less favourable case” of pure  
602        longitudinal or transverse going tracks, it represents a the track length of  $L_{track} \geq$   
603         $4 \times$  scintillator space = 10.0 cm.
- 604        • In the views where particles pass the length criterion, the particle shall not  
605        be superimposed with longer tracks in at least two views. The superposition  
606        criterion is estimated with the distance inter-tracks (DIT) which corresponds to  
607        the orthogonal distance between two tracks at the ending point of the shortest  
608        one (see Figure 30). For a track 1, the superposition criterion is tested with  
609        every longer tracks that starts at the same vertex. Let  $\vec{p}_1$  the vector of track  
610        1, and  $p_1^a$  its projections in the XZ, YZ and XY planes respectively for  $i=1,2,3$ .  
611        Note that these are projections in a 2D planes and not on a direction vector. In  
612        this case, the relative angle between the track 1 and a longer track 2 (of vector  
613         $\vec{p}_2$ ) in a view  $a$  is given by:

$$\cos \theta = \frac{\vec{p}_1^a \cdot \vec{p}_2^a}{\|\vec{p}_1^a\| \|\vec{p}_2^a\|} \quad (2)$$

614

and the distance inter track is given by:

$$DIT = \|\vec{p}_1^a\| \sin \theta \quad (3)$$

615

616        The DIT should be higher than  $4 \times$  scintillator width for the track 1 to be not  
617        superimposed with the track 2 in the view  $a$ , which also corresponds to 10.0 cm  
in the nominal configuration.

618 **6.1.2 Performances**

619 The particle-only reconstruction efficiencies and the reconstruction threshold in momenta  
 620 are shown in Table 7. This threshold is defined as the maximal momentum for which the  
 621 reconstruction efficiency is smaller than 30%. The thresholds in muon and pion momenta  
 622 are 150 MeV/c. Most of the muons are above this threshold (see Figure 29) which leads  
 623 to a 79% reconstruction efficiency.

|                           | $\mu$     | $\pi$     | p         |
|---------------------------|-----------|-----------|-----------|
| Reconstruction Efficiency | 79%       | 52%       | 26%       |
| Momentum threshold        | 150 MeV/c | 150 MeV/c | 550 MeV/c |

Table 7: Reconstruction efficiency and momentum threshold for muons, pions and protons. The threshold is defined as the maximal momentum for which particles have a reconstruction efficiency smaller than 30%.

624 The lower pion and proton efficiencies (respectively 52% and 26%) are due to lower  
 625 efficiencies for similar momenta than muons, coming from strong interactions as shown  
 626 on Figures 31. Efficiencies of each particle type tend to decrease in the backward region  
 627 due to particle lower momenta. However, for a fixed momentum value, the reconstruction  
 628 efficiency is almost uniform which confirms the ability of the WAGASCI detector to  
 629 reconstruct high angle tracks.

630 The reconstruction is thereafter tested on neutrino events. Table 8 summarizes the  
 631 number of reconstructed events and efficiencies for each interaction type. As expected  
 632 from the high muon reconstruction efficiency, the charged current interactions have recon-  
 struction efficiencies  $\geq 85\%$ .

|                           | CC0 $\pi$ | CC1 $\pi$ | CCOthers | NC  | All |
|---------------------------|-----------|-----------|----------|-----|-----|
| Reconstruction efficiency | 85%       | 87%       | 91%      | 22% | 68% |

Table 8: Number of true interactions reconstructed. The purity and reconstruction effi-  
 ciency of each true interaction is also shown.

633  
 634 The reconstruction efficiencies as a function of the neutrino energy and muon kinematics  
 635 are respectively shown on Figure 32 and 33.

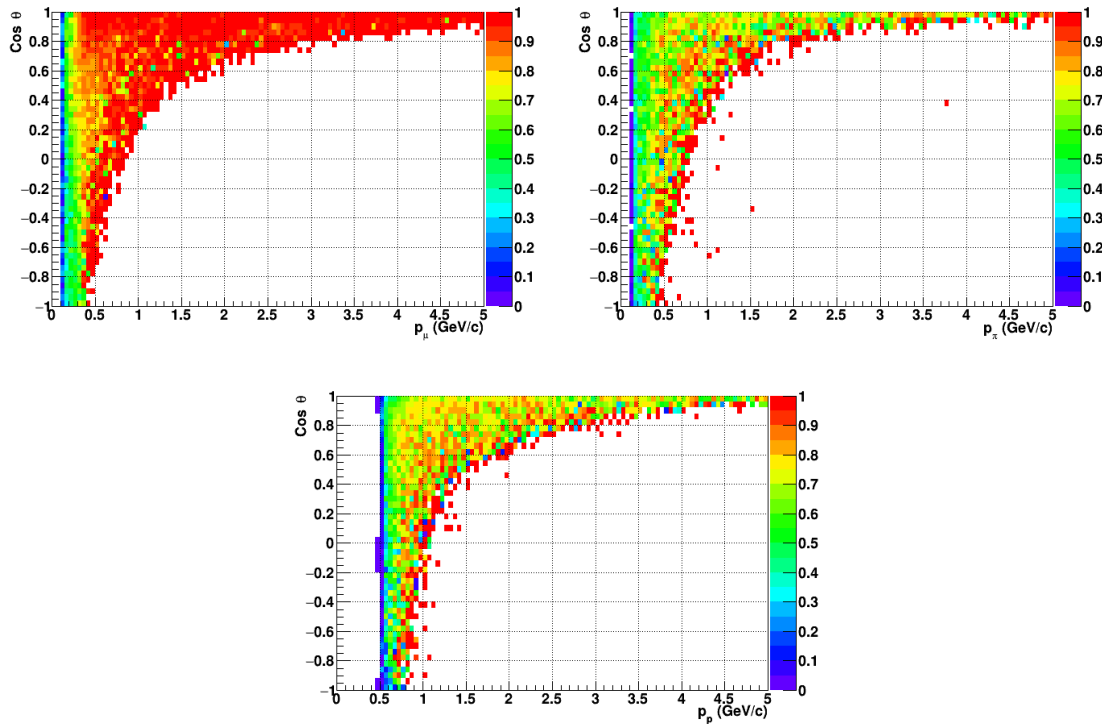


Figure 31: Reconstruction efficiency of muons (left), charged pions (right) and protons (bottom) in the WAGASCI water-module as a function of the particles momenta and angles.

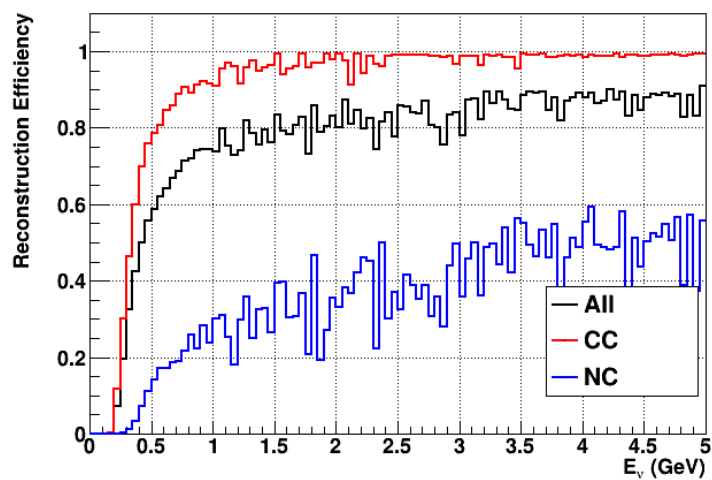


Figure 32: Reconstruction efficiency of all neutrino (black), CC (red) and NC (blue) interactions in the WAGASCI water-module as a function of the neutrino energy.

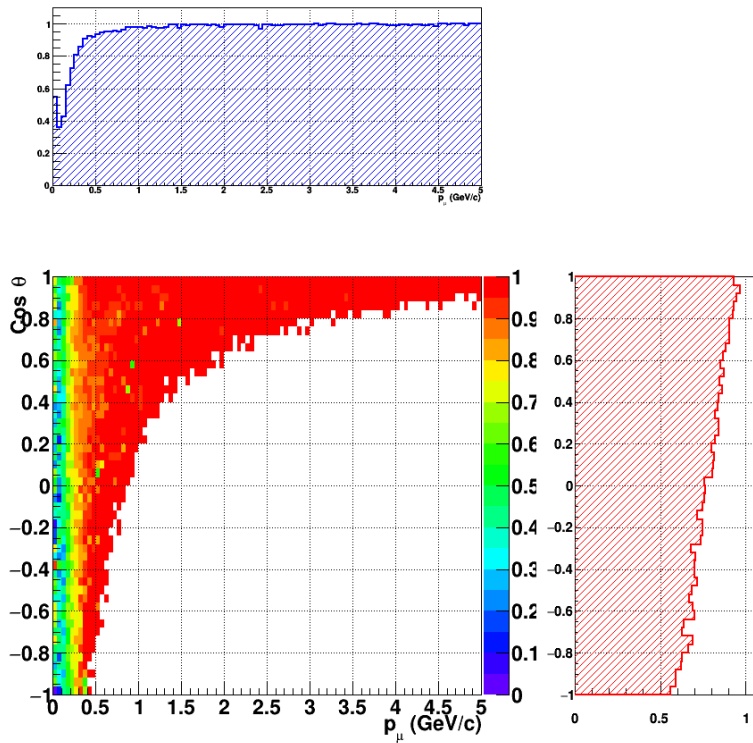


Figure 33: Reconstruction efficiency of CC interactions in the WAGASCI water-module as a function of the muon kinematic variables (momentum and angle).

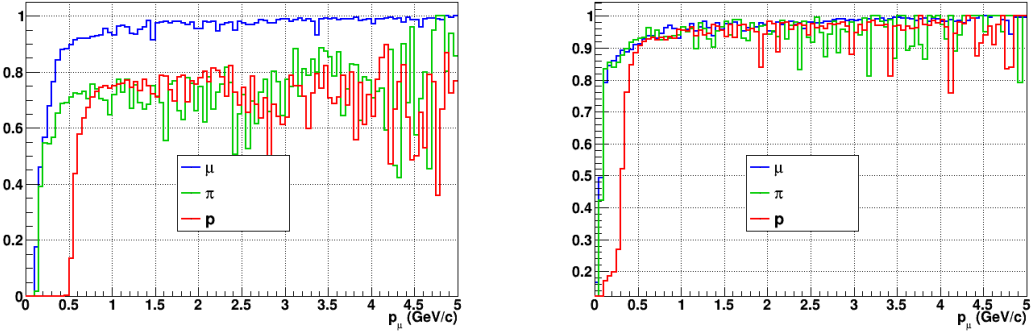


Figure 34: Reconstruction efficiency for muons, pions and protons in the water-in (left) and water-out (right) modules.

636 Note that a Particle Identification Algorithm has been also developed. It is based on  
 637 the charge deposition of the particles in the scintillator, of the detection of a decay-electron.  
 638 However, this information highly depends on the number of scintillator hit by a particle,  
 639 which creates an important difference between a real WAGASCI module and the one used  
 640 for the ND280-upgrade simulation. For this reason, the corresponding results will not be  
 641 detailed here, but can be found in [?].

## 642 6.2 Background subtraction: the water-out module

643 In the nominal configuration, 20% of the neutrino interactions occurs on scintillators  
 644 ( $C_8H_8$ ). This background should be removed in order to measure the neutrino interac-  
 645 tion on the same target as Super-K, which suppress the differences in cross-section models.  
 646 For this purpose, we propose to use a water-out module, where the water is replaced by  
 647 air. The detector is therefore fully active and has a 3 mm spatial resolution (scintillator  
 648 thickness) which create an ideal detector to reconstruct and identify hadrons, and study  
 649 np-nh interactions. The counter-part is the difference in particle energy deposition between  
 650 the water and this water-out module that will need to be corrected for. In this section,  
 651 we present the capabilities of such a module, and the impact it can have on cross-section  
 652 measurements for the neutrino community in general and T2K in particular.  
 653 The same reconstruction and selection as the water-in module is applied. Figure 34 shows  
 654 the comparison between the water-in and the water-out reconstruction efficiencies for muon,  
 655 pions and protons. 90% of the muons and 87% of the pions are reconstructed, while 70%  
 656 of the protons are even reconstructed. It allows to lower down the proton threshold to  
 657 250 MeV/c (see Table 9).

658 As a consequence of tracking even low momenta particle, the reconstruction efficiency  
 659 is uniform and almost maximal on the entire  $\cos \theta_\mu$  phase space, as shown on Figure 35.

|                                                 | $\mu$           | $\pi$           | p                |
|-------------------------------------------------|-----------------|-----------------|------------------|
| Reconstruction Efficiency<br>Momentum threshold | 90%<br>50 MeV/c | 87%<br>50 MeV/c | 70%<br>250 MeV/c |

Table 9: Reconstruction efficiency, proportions of  $\mu$ -like and non  $\mu$ -like and momentum threshold for muons, pions and protons in the empty module. The threshold is defined as the maximal momentum for which particles have a reconstruction efficiency smaller than 20%.

660 Since the fiducial mass represents 0.25 tons, the total number of events is divided by a  
 661 factor of 3 compared to the water-in module. The water-out module offers interesting  
 662 possibilities to study np-nh interaction since 70% of the protons are reconstructed. In the  
 663 future, a possible separation as a function of the number of proton track will be studied.  
 664 Moreover, we are currently pursuing the use of single and double transverse variables (cite  
 665 Xianguo) to open new possibilities for separating np-nh from Final State Interactions, or  
 666 for isolating the interactions on hydrogen from interactions on carbon in this module.

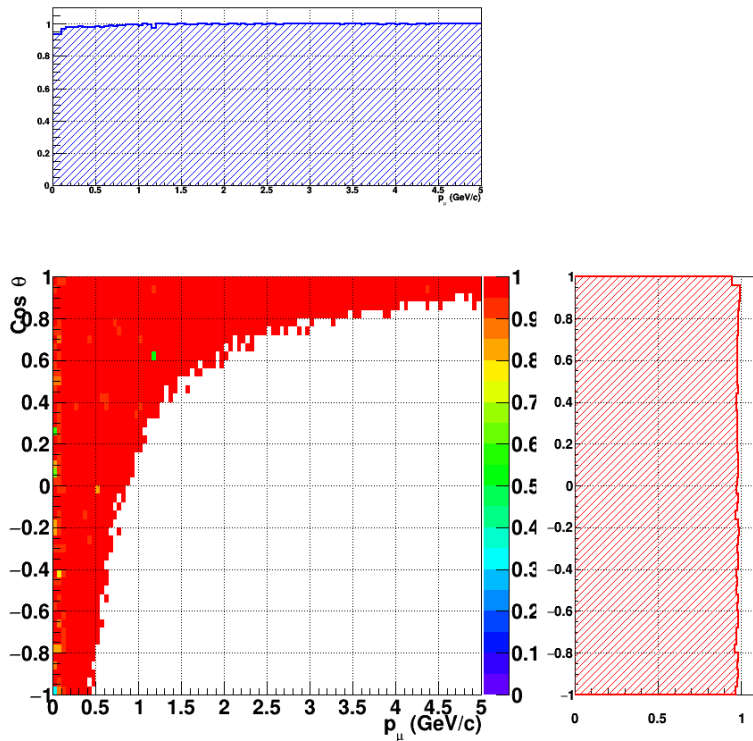


Figure 35: Reconstruction efficiency of CC interactions in the WAGASCI empty module as a function of the muon kinematic variables (momentum and angle).

667 **7 Schedule**

668 We would like to start a physics data taking from T2K beam time after the summer  
669 shutdown in 2018. By then, commissioning and tests of the detectors will be completed  
670 in J-PARC T59. The experiment can run parasitically with T2K, therefore we request no  
671 dedicated beam time nor beam condition as discussed in the following section.

672 Once the approved POT is accumulated, the WAGASCI modules will be removed  
673 from the experimental site, but we would like to keep the Baby-MIND and the Side-MRD  
674 modules on the B2 floor of the NM pit as common platforms of future neutrino experiments  
675 using the T2K neutrino beam.

676 **8 Requests**

677 **8.1 Neutrino beam**

678 The experiment can run parasitically with T2K, therefore we request no dedicated beam  
679 time nor beam condition. As data taking periods, we request the ‘nominal’ T2K one-year  
680 operation both for the neutrino beam and the antineutrino beam. The T2K has been  
681 requesting  $0.9 \times 10^{21}$  POT/year and actually accumulating about  $0.7 \times 10^{21}$  POT/year in  
682 recent years. For each year, starting from the Autumn, T2K is running predominantly in  
683 the neutrino mode or in the antineutrino mode. Our request is to have one-year neutrino-  
684 mode data and another one-year antineutrino mode data assuming that the POT for the  
685 fast extraction in each year is more than  $0.5 \times 10^{21}$  POT.

686 **8.2 Equipment request including power line**

687 We request the followings in terms of equipment on the B2 floor:

- 688 • Site for the WAGASCI modules, Side-MRD modules and BabyMIND and their elec-  
689 tronics system on the B2 floor of the near detector hall (Fig. 2 and 3).
- 690 • Anchor points (holes) on the B2 floor to secure the WAGASCI modules, Side-MRD  
691 module and Baby-MIND, detailed floor plans to be communicated in a separate  
692 document.
- 693 • Power line for the magnets in Baby-MIND: 400 V tri-phase 48-to-62 Hz, capable of  
694 delivering 12 kW. We have a wish for the magnet power line to be installed and  
695 available to us by beginning of March 2018.
- 696 • Electricity for electronics and water circulation system, 3 kW, standard Japanese  
697 electrical sockets.

- 698 1. Online PCs: 2.1 kW

699            2. Electronics: 0.7 kW

700            3. Water sensors: 1 kW

- 701            • Air conditioner for cooling heat generation at Baby-MIND magnets, online PCs and  
702            electeronics
- 703            • Beam timing signal and spill information
- 704            • Network connection

705            The infrastructure for much of the above exists already. Exceptions are the power line  
706            for the magnet and the electronics and holes in the B2 floor to anchor the detector support  
707            structures.

## 708            References

- 709        [1] K. Abe et al. Measurement of the muon neutrino inclusive charged-current cross  
710            section in the energy range of 13 GeV with the T2K INGRID detector. *Phys. Rev.*,  
711            D93(7):072002, 2016.
- 712        [2] M. Antonova et al. Baby MIND Experiment Construction Status. In *Prospects in*  
713            *Neutrino Physics (NuPhys2016) London, London, United Kingdom, December 12-14,*  
714            2016, 2017.
- 715        [3] K. Nitta et al. The k2k scibar detector. *Nucl. Instrum. Meth. A*, 535:147, 2004.
- 716        [4] K. Abe et al. (T2K Collaboration). Measurement of the inclusive  $\nu_\mu$  charged current  
717            cross section on iron and hydrocarbon in the t2k on-axis neutrino beam. *Phys. Rev.*  
718            D, 90:052010, 2014.
- 719        [5] F. Magniette F. Gastaldi, R. Cornat and V. Boudry. A scalable gigabit data acquisition  
720            system for calorimeters for linear collider. *proceedings of TIPP2014*, page PoS 193,  
721            2014.
- 722        [6] J. Fleury, S. Callier, C. de La Taille, N. Seguin, D. Thienpont, F. Dulucq, S. Ahmad,  
723            and G. Martin. Petiroc and Citiroc: front-end ASICs for SiPM read-out and ToF  
724            applications. *JINST*, 9:C01049, 2014.
- 725        [7] M. B. Barbaro J. A. Caballero T. W. Donnelly G. D. Megias, J. E. Amaro. Inclusive  
726            electron scattering within the susav2 meson-exchange current approach. *Phys. Rev.*  
727            D, 94:013012, 2016.
- 728        [8] M. Valverde J. Nieves, J. E. Amaro. Inclusive quasi-elastic neutrino reactions. *Phys.*  
729            *Rev. C*, 70:055503, 2004.

- 730 [9] Yu. G. Kudenko, L. S. Littenberg, V. A. Mayatsky, O. V. Mineev, and N. V. Ershov.  
731 Extruded plastic counters with WLS fiber readout. *Nucl. Instrum. Meth.*, A469:340–  
732 346, 2001.
- 733 [10] O. Mineev, Yu. Kudenko, Yu. Musienko, I. Polyansky, and N. Yershov. Scintillator  
734 detectors with long WLS fibers and multi-pixel photodiodes. *JINST*, 6:P12004, 2011.
- 735 [11] Etam Noah et al. Readout scheme for the Baby-MIND detector. *PoS*, Photo-  
736 toDet2015:031, 2016.
- 737 [12] Omega. Spiroc 2 user guide. 2009.